

Reverse Engineering of Generative Models: Inferring Model Hyperparameters from Generated Images

Vishal Asnani , Xi Yin, Tal Hassner, Xiaoming Liu

Abstract—State-of-the-art (SOTA) Generative Models (GMs) can synthesize photo-realistic images that are hard for humans to distinguish from genuine photos. We propose to perform reverse engineering of GMs to infer the model hyperparameters from the images generated by these models. We define a novel problem, “model parsing”, as estimating GM network architectures and training loss functions by examining their generated images – a task seemingly impossible for human beings. To tackle this problem, we propose a framework with two components: a Fingerprint Estimation Network (FEN), which estimates a GM fingerprint from a generated image by training with four constraints to encourage the fingerprint to have desired properties, and a Parsing Network (PN), which predicts network architecture and loss functions from the estimated fingerprints. To evaluate our approach, we collect a fake image dataset with 100K images generated by 100 GMs. Extensive experiments show encouraging results in parsing the hyperparameters of the unseen models. Finally, our fingerprint estimation can be leveraged for deepfake detection and image attribution, as we show by reporting SOTA results on both the recent Celeb-DF and image attribution benchmarks.

Index Terms—Reverse Engineering, Fingerprint Estimation, Generative Models, Deepfake Detection, Image Attribution

1 INTRODUCTION

Image generation techniques have improved significantly in recent years especially after the breakthrough of Generative Adversarial Networks (GANs) [1]. Many Generative Models (GMs), including both GAN and Variational Autoencoder (VAE) [2], [3], [4], [5], [6], [7], can generate photo-realistic images that are hard for human to distinguish from genuine photos. This photo-realism, however, raises increasing concerns for the potential misuse of these models, *e.g.*, by launching coordinated misinformation attack [8], [9]. As a result, deepfake detection [10], [11], [12], [13], [14], [15] has recently attracted increasing attention. Going beyond the binary genuine *vs.* fake classification as in deepfake detection, Yu *et al.* [16] proposed source model classification given a generated image. This *image attribution* problem assumes a *closed set* of GMs, used in both training and testing.

It is desirable to generalize image attribution to open-set recognition, *i.e.*, classify an image generated by GMs which were *not* seen during training. However, one may wonder what else can we do beyond recognizing a GM as an *unseen* or *new* model. Can we know more about how this new GM was designed? How its architecture differs from known GMs in the training set? Answering these questions is valuable when we, as defenders, strive to understand the source of images generated by malicious attackers or identify coordinated misinformation attacks [8], [9] which use the same GM. We view this as the grand challenge of reverse engineering of GMs.

While image attribution of GMs is both exciting and challenging, our work aims to take one step further with the following observation. When different GMs are designed, they mainly differ in their model hyperparameters, including the network architectures (*e.g.*, the number of layers/blocks, the type of normalization) and

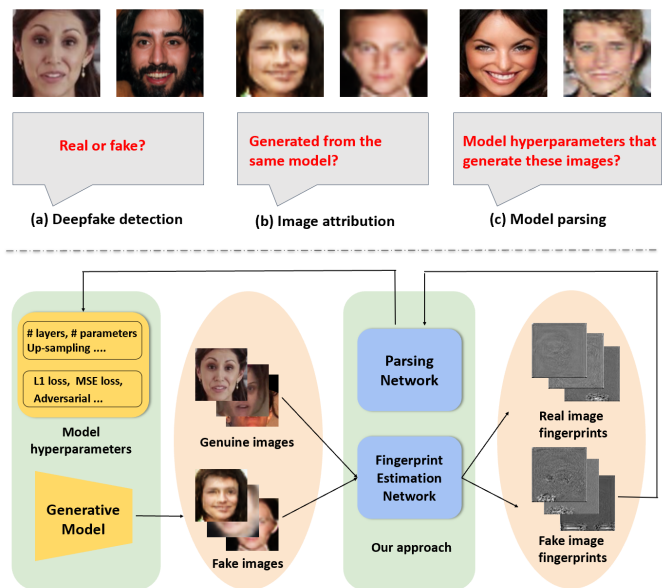


Fig. 1: Top: Three increasingly difficult tasks: (a) *deepfake detection* classifies an image as genuine or fake; (b) *image attribution* predicts which of a closed set of GMs generated a fake image; and (c) *model parsing*, proposed here, infers hyperparameters of the GM used to generate an image, for those models unseen during training. Bottom: We present a framework for model parsing. This framework can also be used to solve the simpler tasks of deepfake detection and image attribution.

training loss functions. If we could map the generated images to the embedding space of model hyperparameters used to generate them, there is a potential to tackle a new problem termed *model parsing*, *i.e.*, estimating hyperparameters of an *unseen* GM from only its generated image (Figure 1). Reverse engineering machine

learning models has been done before by relying on a model’s input and output [17], [18], or accessing the hardware usage during inference [19], [20]. To the best of our knowledge, however, reverse engineering has never been explored for GMs, especially with only generated images as input.

There are many publicly available GMs that generate images in diverse contents, including faces, digits, and generic objects. Our framework is not specific to a particular content. To improve the generalization of model parsing, we collect a large-scale fake image dataset. It consists of images generated from 100 GMs, including 81 GANs, 13 VAEs and 6 Adversarial Attack models (AAs). While GAN or VAE generates an image by feeding a genuine image or latent code through the network, the AA model modifies a genuine image based on its objectives through back-propagation. Despite this difference, we call all these models as GMs for simplicity. Each GM generates 1,000 images, which are included in our dataset. We use each model’s hyperparameters, including network architecture parameters and training loss types, as the ground-truth for model parsing training. We propose a framework to peek inside the black boxes of these GMs by estimating their hyperparameters from the generated images. Unlike the closed set setting in [16], we venture into quantifying the generalization ability of our method in parsing *unseen* GMs.

Our framework consists of two components (Figure 1, bottom). A *Fingerprint Estimation Network* (FEN) infers the subtle yet unique patterns left by GMs on their generated images. Image fingerprint was first applied to images captured by conventional cameras [21], [22], [23], [24], [25], [26], [27] and then extended to GMs [16], [28]. We estimate fingerprints using different constraints which are based on the properties of fingerprint in general, including the fingerprint magnitude, repetitive nature, frequency range and symmetrical frequency response. Different loss functions are defined to apply these constraints in FEN, so that the generated fingerprints can have these desired properties. These constraints enable us to estimate fingerprints of GMs without ground truth.

The estimated fingerprints are discriminative and can serve as the cornerstone for subsequent tasks. The second part of our framework is a *Parsing Network* (PN), which takes the fingerprint as input and predicts the model hyperparameters. We consider parameters representing network architectures and loss function types. For network architectures, we form 15 parameters and categorize them into discrete and continuous types. Classification is used for estimating discrete parameters like the normalization type, and regression is used for continuous parameters like the number of layers. For loss function type prediction, we group nine different loss functions into three categories in a novel hierarchical learning, designed to make training easier.

We partition all GMs into two categories: face vs. non-face. Among the 100 GMs in our collected dataset, there are 47 models for face generation and 53 for non-face image generation. We carefully curate six evaluation sets for face and non-face categories respectively. Each evaluation set is formulated to be representative of the GM population. Cross validation is used in our experiments. In addition to model parsing, our FEN can be used for deepfake detection and image attribution. For both tasks, we add a shallow network that inputs the estimated fingerprint and performs binary (deepfake detection) or multi-class classification (image attribution). Although our FEN is not tailored for these tasks, we still achieve state-of-the-art (SOTA) performance, indicating the superior generalization ability of our fingerprint estimation.

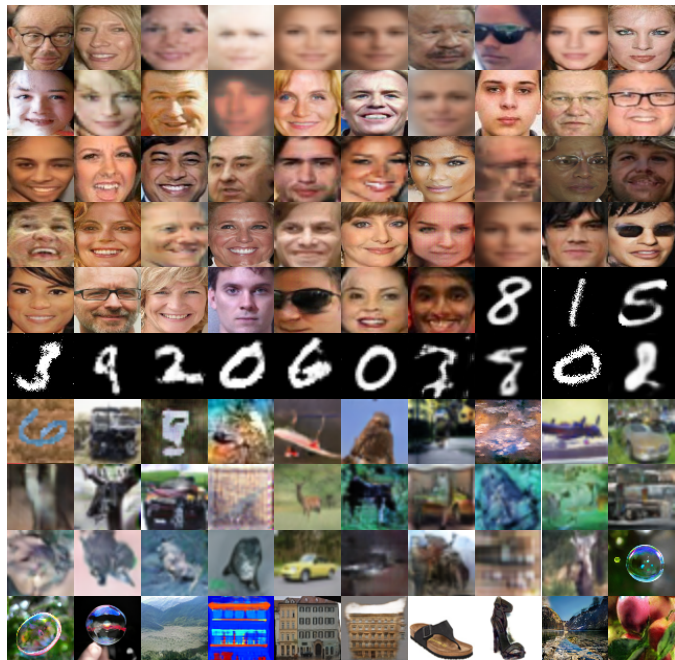


Fig. 2: Example images generated by all 100 GMs in our collected dataset (one image per model). To ensure that the reverse engineering is content independent, our testing sets contain either only face images or only non-face images.

In summary, this paper makes the following contributions.

- We are the first to go beyond model classification by formulating a novel problem of model parsing for GMs.
- We propose a novel framework with fingerprint estimation to predict the network architecture and loss functions, given a single generated image.
- We assemble a dataset of generated images from 100 GMs, including ground-truth labels on the network architectures and loss function types.
- We show that our approach generalizes well to tasks of deepfake detection on the Celeb-DF benchmark [29] and image attribution [16], in both cases reporting results comparable or better than existing SOTA [14], [16].

2 RELATED WORK

Reverse engineering of models. It is a growing area of interest to reverse engineering the hyperparameters of machine learning models. There are two types of approaches. First, some methods treat a model as a black box API by examining its input and output pairs. For example, Tramer *et al.* [17] developed an avatar method to estimate training data and model architectures, while Oh *et al.* [18] trained a set of white-box models to estimate model hyperparameters. The second type of approaches assumes that the intermediate hardware information is available during model inference. Hua *et al.* [19] estimated both the structure and the weights of a CNN model running on a hardware accelerator, by using information leaks of memory access patterns. Batina *et al.* [20] proposed to estimate the network architecture by using side-channel information such as timing and electromagnetic emanations.

Unlike prior methods which require access to the models or their inputs, our approach can reverse engineer GMs by examining

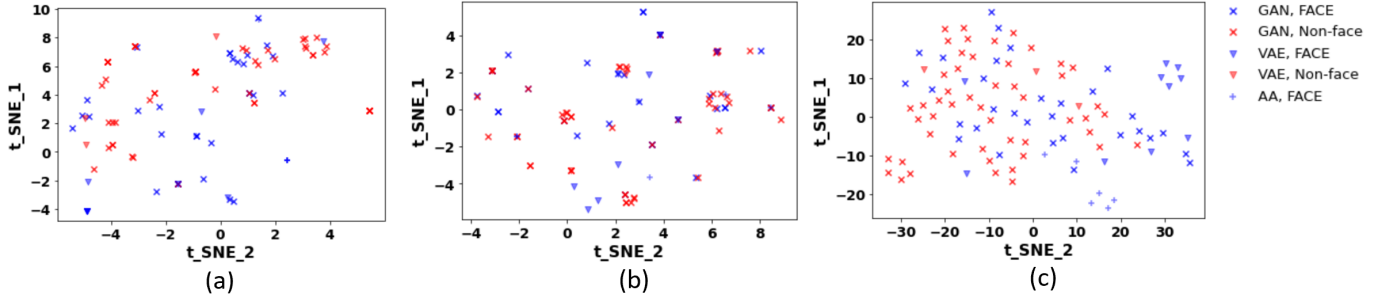


Fig. 3: t_SNE visualization for ground-truth feature vectors for (a) network architecture, (b) fine-level loss function and (c) network architecture and fine-level loss function combined. The ground-truth feature vectors are fairly distributed across the feature space regardless of the face/non-face data.

only the images generated by these models, making it more suitable for real-world applications.

Fingerprint estimation. Every acquisition device leaves a subtle but unique pattern on each image, due to manufacturing imperfections. Such patterns are referred to as *device fingerprints*. Device fingerprint estimation [21], [30] was extended to fingerprint estimation of GMs by Marra *et al.* [28], who showed that hand-crafted fingerprints are unique to each GM and can be used to identify an image’s source. Ning *et al.* [16] extended this idea to learning-based fingerprint estimation. Both methods rely on the noise signals in the image. Others explored frequency domain information. For example, Wang *et al.* [31] showed that CNN generated images have unique patterns in the frequency domain, regarded as model fingerprints. Zhang *et al.* [32] showed that features extracted from the middle and high frequencies of the spectrum domain were useful in detecting upsampling artifacts produced by GANs.

Unlike prior methods which derive fingerprints directly from noise signals or the frequency domain, we propose several novel loss functions to learn GM fingerprints. We further show that our fingerprint estimation can generalize well to other related tasks.

Deepfake detection. Deepfake detection is a very active new field with many recent developments. Rossler *et al.* [10] evaluated different methods for detecting face and mouth replacement manipulation. Others proposed SVM classifier on colour difference features [11]. Guarnera *et al.* [12] used Expectation Maximization [33] algorithm to extract features and convolution traces for classification. Marra *et al.* [13] proposed a multi-task incremental learning to classify new GAN generated images. Chai *et al.* [34] introduced a patch-based classifier to exaggerate regions that are more easily detectable. An attention mechanism [35] was proposed by Hao *et al.* [14] to improve the performance of deepfake detection. Finally, Nirkin *et al.* [15] seek discrepancies between face regions and their context [36] as telltale signs of manipulation. In our work, the estimated fingerprint is fed into a classifier for genuine vs. fake classification.

3 PROPOSED APPROACH

In this section, we first introduce our collected dataset in Sec. 3.1. We then present the fingerprint estimation method in Sec. 3.2 and model parsing in Sec. 3.3. Our estimated fingerprints can be leveraged for deepfake detection and image attribution, as described in Sec. 3.4.

3.1 Data collection

We make a first attempt to study the model parsing problem. Since data drives research, it is important to collect a dataset for our new research problem. Given the large number of GMs published in recent years [37], [38], we consider a few factors while deciding which GMs to be included in our dataset. First of all, since it is desirable to study if model parsing is content dependent, we would like to collect GMs with as diverse content as possible, such as face, digits, and generic objects. Secondly, we give preference to GMs where either the authors have released pre-trained models/images or there is a training script available publicly to train models from scratch. Third, the network architecture of the GM should be clearly described in the respective paper.

To this end, we assemble a list of 100 GMs, including ProGAN [4], StyleGAN [2], and others (a full list is provided in the supplementary material). For each GM, we collect 1,000 generated images. We show example images in Figure 2. These GMs were trained on datasets with a variety of contents, such as CelebA [39], MNIST [40], CIFAR10 [41], ImageNet [42], facades [43], edges2shoes [43] and apple2oranges [43].

For each GM, we further document the model hyperparameters as reported in their papers. Specifically, we investigate two aspects: network architecture and training loss functions. We form a super-set of 15 network architecture parameters, (*e.g.*, number of layers, normalization type) and eight different loss function types. We consequently obtain a large-scale fake image dataset $\mathbb{D} = \{\mathbf{X}_i, \mathbf{y}_i^n, \mathbf{y}_i^l\}_{i=1}^N$ where $\mathbf{X}_i \in \mathbb{R}^{64 \times 64 \times 3}$ is a fake image, $\mathbf{y}_i^n \in \mathbb{R}^{15}$ and $\mathbf{y}_i^l \in \mathbb{R}^8$ are the vectors representing the ground-truth network architecture and loss functions, respectively. We also show the t-SNE distribution for both network architecture and loss functions in Figure 3 for different type of models and datasets. We can clearly observe that ground-truth vectors both for network architecture and loss function are evenly distributed across the space for both type of data: face and non-face.

3.2 Fingerprint estimation

We adopt a network structure similar to the DnCNN model used in [44]. As shown in Figure 4, the input to FEN is a generated image \mathbf{X} , and the output is a fingerprint image \mathbf{F} of the same size. Motivated from prior works on physical fingerprint estimation [16], [28], [31], [32], [45], we define the following four constraints to guide our estimated fingerprints to have desirable properties.

Magnitude loss. Fingerprints can be considered as image noise patterns with small magnitude. Similar assumptions were made by

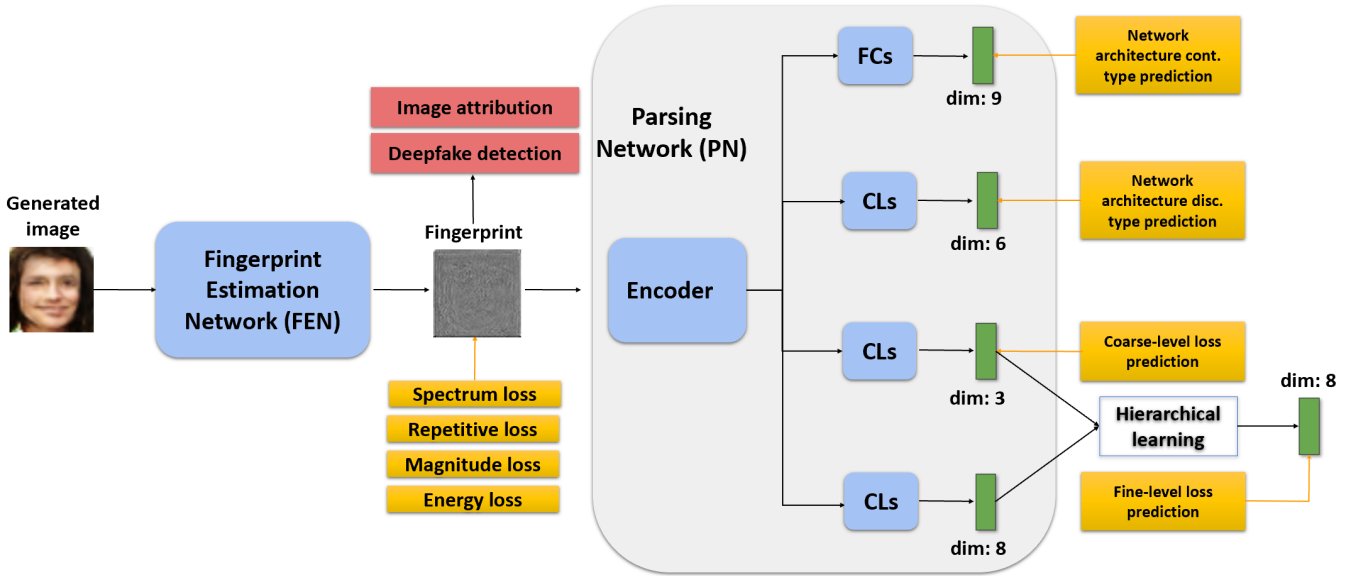


Fig. 4: Our framework includes two major components: 1) the FEN is trained with four objectives for fingerprint estimation; and 2) the PN consists of a shared encoder, fully connected layers (FCs) for continuous type parameters in network architecture and three separate classifiers (CLs) for discrete type parameters in network architecture and loss function prediction. We propose a hierarchical learning scheme for loss function prediction. In this figure, blue boxes denote trainable components; green boxes denote feature vectors; orange boxes denote loss functions; red boxes denote other tasks our framework can handle; black arrows denote data flow; orange arrows denote loss supervisions. Best viewed in color.

TABLE 1: Hyper-parameters representing the network architectures of the 100 GMs. We use abbreviations for space concern. (cont. int.: continuous integer.)

Parameter	Type	Range	Parameter	Type	Range	Parameter	Type	Range
# layers	cont. int.	[5, 95]	# filter	cont. int.	[0, 8365]	non-linearity type in blocks	multi-class	0, 1, 2, 3
# convolutional layers	cont. int.	[0, 92]	# parameters	cont. int.	[0.36M, 267M]	non-linearity type in last layer	multi-class	0, 1, 2, 3
# fully connected layers	cont. int.	[0, 40]	# blocks	cont. int.	[0, 16]	up-sampling type	binary	0, 1
# pooling layers	cont. int.	[0, 4]	# layers per block	cont. int.	[0, 9]	skip connection	binary	0, 1
# normalization layers	cont. int.	[0, 57]	normalization type	multi-class	0, 1, 2, 3	down-sampling	binary	0, 1

others when estimating spoof noise for spoofed face images [45] and sensor noise for genuine images [21]. The first constraint is thus proposed to regularize the fingerprint image to have low magnitude with a L_2 loss:

$$J_m = \|\mathbf{F}\|_2^2. \quad (1)$$

Spectrum loss. Previous work observed that fingerprints mostly lie in the middle and high frequency bands of an image [32]. We thus propose to minimize the low frequency content in a fingerprint image by applying a low pass filter to its frequency domain:

$$J_s = \|\mathcal{L}(\mathcal{F}(\mathbf{F}), k)\|_2^2, \quad (2)$$

where \mathcal{F} is the Fourier transform, \mathcal{L} is the low pass filter selecting the $k \times k$ region in the center of the 2D Fourier spectrum and making everything else zero.

Repetitive loss. Amin *et al.* [45] noted that the noise characteristics of an image are repetitive and exist everywhere in its spatial domain. Such repetitive patterns will result in large magnitude in the high frequency band of the fingerprint. Therefore, we propose to maximize the high frequency information in order to encourage this repetitiveness pattern:

$$J_r = -\max\{\mathcal{H}(\mathcal{F}(\mathbf{F}), k)\}, \quad (3)$$

where \mathcal{H} is a high pass filter assigning the $k \times k$ region in the center of the 2D Fourier spectrum to zero.

Energy loss : Wang *et al.* [31] showed that unique patterns exist in the Fourier spectrum of the image generated by CNN networks. These patterns have similar energy in the vertical and horizontal direction of the Fourier spectrum. Our final constraint is proposed to incorporate this observation:

$$J_e = \|\mathcal{F}(\mathbf{F}) - \mathcal{F}(\mathbf{F})^T\|_2^2, \quad (4)$$

where $\mathcal{F}(\mathbf{F})^T$ is the transpose of $\mathcal{F}(\mathbf{F})$.

These constraints guide the training of our fingerprint estimation. The overall loss function for fingerprint estimation is given by:

$$J_f = \lambda_1 J_m + \lambda_2 J_s + \lambda_3 J_r + \lambda_4 J_e, \quad (5)$$

where $\lambda_1, \lambda_2, \lambda_3, \lambda_4$ are the loss weights for each term.

3.3 Model parsing

The estimated fingerprint is expected to capture unique patterns generated from GM. Prior works adopted fingerprint for deepfake detection [11], [12] and image attribution [16]. We go beyond those efforts by parsing the hyperparameters of GMs. As shown in Figure 4, the parsing network consists of a shared encoder and separate branches for network architecture and loss function prediction.

TABLE 2: Loss function types used by all GMs. We group the eight loss functions into three categories, which enable us to develop a hierarchical learning scheme for loss function prediction.

Category	Loss function
Pixel-level	L_1
	L_2
	Mean squared error (MSE)
Discriminator	Maximum mean discrepancy (MMD)
	Wasserstein loss for GAN (WGAN)
	Kullback–Leibler (KL) divergence
Classification	Adversarial
	Cross-entropy (CE)

3.3.1 Network architecture prediction

In this work, we do not aim to recover the network parameters. The reason is that a typical deep network has millions of network parameters, which reside in a very high dimensional space and is thus hard to predict. Instead, we propose to infer the hyperparameters that define the network architecture, which is much fewer than the network parameters. Motivated by literatures in neural architecture search [46], [47], [48], we form a set of 15 network architecture parameters that cover various aspects of GMs. As shown in Tab. 1, these parameters fall into different data types and have different ranges. We further split the network architecture parameters \mathbf{y}^n into two parts: $\mathbf{y}^{n_c} \in \mathbb{R}^9$ for continuous data type and $\mathbf{y}^{n_d} \in \mathbb{R}^6$ for discrete data type.

For continuous parameters, we perform regression for parameter estimation. As these parameters are in different ranges, we further perform a min-max normalization to bring all parameters into the range of [0, 1]. A standard L_2 loss is used to estimate the prediction error:

$$J_{n_c} = \|\hat{\mathbf{y}}^{n_c} - \mathbf{y}^{n_c}\|_2^2, \quad (6)$$

where $\hat{\mathbf{y}}^{n_c}$ is the prediction and \mathbf{y}^{n_c} is the min-max normalized ground-truth network architecture parameters of continuous data type.

For discrete parameters, the prediction is done via individual classifiers for each parameter. We have noticed the class distribution for some parameters is imbalanced. To handle this challenge, we apply the weighted cross-entropy loss for every parameter. Specifically, we train $K = 6$ classifiers; one for each of the discrete parameters. For the k th classifier with M_k classes ($M_k = 2$ or 4 in our case), we calculate a loss weight for each class as $w_k^c = \frac{N}{N_k^c}$ where N_k^c is the number of training examples for the c th class of k th classifier, and N is the number of total training examples. As a result, the class with more examples are down-weighted and class with less examples are up-weighted to overcome the imbalance issue, which will be empirically demonstrated in Figure 9. The loss term for discrete network architecture prediction is defined as:

$$J_{n_d} = - \sum_{k=1}^K \text{sum}(\mathbf{w}_k \odot \mathbf{y}_k^{n_d} \odot \log(\mathcal{S}(\hat{\mathbf{y}}_k^{n_d}))), \quad (7)$$

where $\mathbf{y}_k^{n_d}$ is the ground-truth one-hot vector for the k th classifier, \mathbf{w}_k is a weight vector for all classes in the k th classifier, $\hat{\mathbf{y}}_k^{n_d}$ are the class logits, \mathcal{S} is the Sigmoid function that maps the class logits into the range of [0, 1], \odot is the element-wise multiplication, and $\text{sum}()$ computes the summation of a vector’s elements.

The overall loss function for network architecture prediction is given by:

$$J_n = J_{n_c} + J_{n_d}. \quad (8)$$

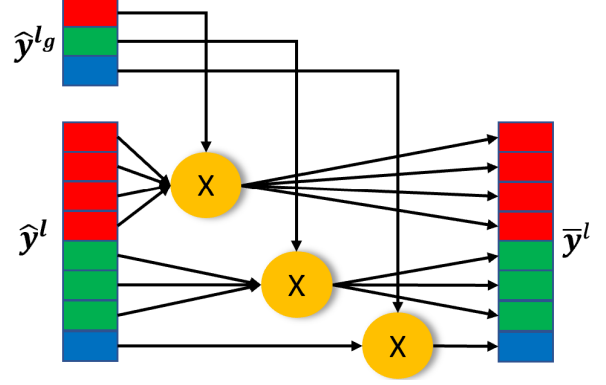


Fig. 5: Hierarchical learning for loss function prediction. The classification probability of each loss term, $\hat{\mathbf{y}}^l$, is multiplied by the classification probability of its corresponding category in $\hat{\mathbf{y}}^{lg}$.

3.3.2 Loss function prediction

In addition to the network architectures, the learned network parameters of trained GM can also impact the fingerprints left on generated images. These network parameters are mostly determined by the training data and the loss functions used to train these models. We therefore explore the possibility of predicting also the training loss functions from the estimated fingerprints.

The 100 GMs were trained with eight types of loss functions. For each model, we compose a ground-truth vector $\mathbf{y}^l \in \mathbb{R}^8$, where each element is a binary value indicating whether the corresponding loss is used or not in training this model. We find that directly classifying these eight loss functions, independently, does not produce satisfactory results. We hypothesize that some of these loss functions might be too fine-grained to be easily distinguished. We therefore propose grouping these eight loss functions into three categories to ease training. As shown in Tab. 2, these three categories include:

- 1) Pixel-level loss.** It includes L_1 , L_2 , mean square error, and maximum mean discrepancy. These loss functions are applied directly to the pixel values of the generated images, enforcing the similarity to genuine images.
- 2) Discriminator loss.** It consists of Wasserstein GAN loss, KL divergence loss, and adversarial loss. These loss functions are applied with a discriminator that distinguishes between genuine and fake images. The goal of this discriminator loss is to generate realistic images.
- 3) Classification loss.** It includes the cross-entropy loss, which is used to regularize the generated image to have certain properties other than photographic realism.

We find that estimating three loss function groups from the estimated fingerprints is relatively easier. However, three categories are too coarse to characterize 100 GMs. Therefore, we propose a hierarchical learning scheme to perform prediction at coarse- and fine-level, by leveraging the relationships among these loss functions.

We use $\mathbf{y}^l \in \mathbb{R}^8$ and $\mathbf{y}^{lg} \in \mathbb{R}^3$ to denote the ground truth for coarse- and fine-level loss function type parameters. Similar to the discrete network architecture parameters, we also observe imbalanced distributions with the loss function parameters. Therefore, weighted cross-entropy loss is used similar to Eqn. 7. For the

coarse-level parameter predictions, the loss is formulated as:

$$J_{l_g} = - \sum_{m=1}^3 \text{sum}(\mathbf{w}_m^{l_g} \odot \mathbf{y}_m^{l_g} \odot \log(\mathcal{S}(\hat{\mathbf{y}}_m^{l_g}))), \quad (9)$$

where $\mathbf{y}_k^{l_g}$ is the ground-truth one-hot vector for the m th classifier, $\mathbf{w}_m^{l_g}$ is a weight vector for all classes in the m th classifier, and $\hat{\mathbf{y}}_k^{l_g}$ are the class logits.

The fine-level loss function estimation depends on the coarse-level prediction. Hence, if we estimate a very low probability of having pixel-level loss, then the probabilities of all the four loss functions in the pixel-level loss category would have low probabilities. The probability of fine-level prediction can therefore be multiplied by the coarse-level probability. We define the updated probability vector as:

$$\bar{\mathbf{y}}^l = \begin{cases} \mathcal{S}(\hat{\mathbf{y}}^{l_g})_1 \mathcal{S}(\hat{\mathbf{y}}^l)_m, & m \in \{1, 2, 3, 4\}. \\ \mathcal{S}(\hat{\mathbf{y}}^{l_g})_2 \mathcal{S}(\hat{\mathbf{y}}^l)_m, & m \in \{5, 6, 7\}. \\ \mathcal{S}(\hat{\mathbf{y}}^{l_g})_3 \mathcal{S}(\hat{\mathbf{y}}^l)_m, & m \in \{8\}. \end{cases} \quad (10)$$

This idea is illustrated in Figure 5. The loss is applied on the updated probability vector:

$$J_l = - \sum_{m=1}^8 \text{sum}(\mathbf{w}_m^l \odot \mathbf{y}_m^l \odot \log(\mathcal{S}(\bar{\mathbf{y}}_m^l))), \quad (11)$$

where \mathbf{y}_k^l is the ground-truth one-hot vector for the m th classifier, \mathbf{w}_m^l is a weight vector for all classes in the m th classifier, $\hat{\mathbf{y}}_k^l$ are the class logits.

In summary, the overall loss function for the parsing network, including both network architecture estimation and training loss function prediction, is given as:

$$J_p = \gamma_1 J_n + \gamma_2 J_{l_g} + \gamma_3 J_l, \quad (12)$$

where γ_1 , γ_2 , and γ_3 are the loss weights. Our framework is trained end-to-end with both fingerprint estimation (Eqn. 5) and model parsing (Eqn. 12).

3.4 Other applications

In addition to model parsing, our fingerprint estimation can be easily leveraged for other applications such as deepfake detection and image attribution.

Deepfake detection. We consider the binary classification of an image as either genuine or fake. To perform this task, we add a shallow network on the generated fingerprint to predict the probabilities of being genuine or fake. The shallow network consists of five convolutional layers and two fully connected layers. Both genuine and fake face images are used as input to our model. Both FEN and the shallow network are trained end-to-end with the proposed fingerprint constraints (Eqn. 5) and a standard cross-entropy loss for genuine vs. fake classification. Note that the fingerprint constraints (Eqn. 5) are not applied to the genuine input face images.

Image Attribution. We aim to learn a mapping from a given image to the model that generated it if it is fake or classified as genuine otherwise. All models are known during training. We solve image attribution as a classification problem. Similar to deepfake detection, we add a shallow network on the generated fingerprint for model classification with the cross-entropy loss. The shallow network consists of two convolutional layers and two fully connected layers.

4 EXPERIMENTS

4.1 Settings

Dataset. As described in Sec. 3.1, we have collected a fake image dataset consists of 100K images from 100 GMs (1K images per model) for model parsing experiments. These models can be split into two parts: 47 face models and 53 non-face models. We focus our evaluation mainly on face models. Instead of performing one split of training and testing sets, we carefully construct six testing sets of face models. For each set, we select representative models in order to evaluate the generalization ability of our algorithm. Specifically, each face testing set includes three GANs, two VAEs, and one AA model. We perform cross-validation to train on 94 models and evaluate on the remaining 6 models in each face testing set. The performance are averaged across 6 testing sets.

For deepfake detection experiments, we conduct experiments on the recently released Celeb-DF dataset [29], consisting of 590 real and 5,639 fake videos. For image attribution experiments, a source database with genuine images needs to be selected, from which the fake images can be generated by various GAN models. We select two source datasets: CelebA [29] and LSUN [49], for two experiments. From each source dataset, we construct a training set of 100K genuine and 100K fake face images produced by each of the same four GAN models used in Yu *et al.* [16], and a testing set with 10K genuine and 10K fake images per model.

Implementation details. Our framework is trained end-to-end with the loss functions of Eqn. 5 and Eqn. 12. The loss weights are set to make the magnitudes of all loss terms comparable: $\lambda_1 = 0.05$, $\lambda_2 = 0.001$, $\lambda_3 = 0.1$, $\lambda_4 = 1$, $\gamma_1 = 5$, $\gamma_2 = 5$, $\gamma_3 = 5$. The value of k for spectrum loss and repetitive loss in the fingerprint estimation is set to 50. We use Adam optimizer with a learning rate of 0.0001 for FEN and 0.001 for PN. Our framework is trained with a batch size of 128 for 10 epochs. All the experiments are conducted using NVIDIA Tesla K80 GPUs.

Evaluation metrics. For network architecture prediction, we report the L_1 error for the regression estimation of continuous type parameters. As there is imbalance in the dataset for different parameters, we estimate the F1 score [50], [51] for classification performance of discrete type parameters. For loss function type prediction, we also report the F1 score. For all cross-validation experiments, we report the averaged results across all images and all GMs.

Our code and pretrained models are available at https://github.com/vishal3477/Reverse_Engineering_GMs

4.2 Model parsing results

As we are the first to attempt GM parsing, there are no existing baselines for comparison. To provide a baseline, we therefore draw analogy with the image attribution task, where each model is represented as a one-hot vector and different models have equal inter-model distances in the high-dimensional space defined by these one-hot vectors. In model parsing, we represent each model as a 23-D vector consisting of network architectures (15-D) and training loss functions (8-D). Thus, these models are not of equal distance in the 23-D space.

Based on the aforementioned observation, we define a simple baseline, referred here as *random ground-truth*. Specifically, for each parameter, we shuffle the values/classes across all 100 GMs to ensure that the feature vector is different from actual ground-truth feature vector but also preserving the actual distribution

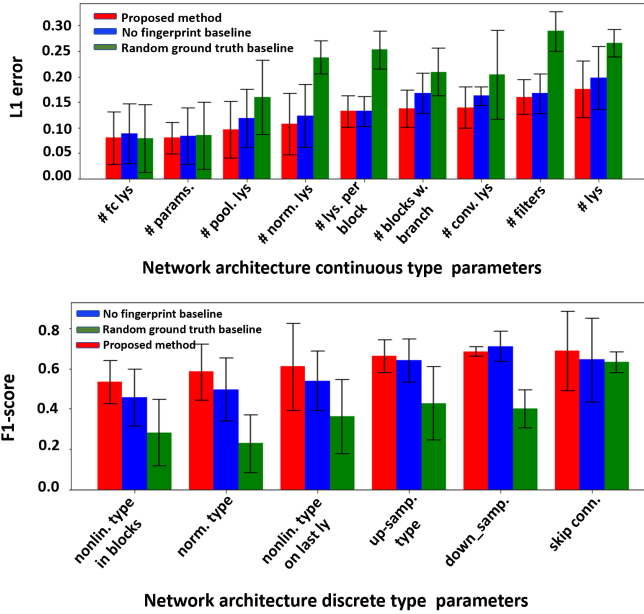


Fig. 6: L_1 error and F1 score for continuous and discrete parameters respectively of network architecture averaged across all images of all models in the 6 test sets. Not only we have better average performance, but also our standard deviations are smaller.

TABLE 3: Performance of network architecture prediction: L_1 error for continuous type parameters and F1 score for discrete type variables. Our method performs better for both type of variables compared to the two baselines.

Method	Continuous type L_1 error \downarrow	Discrete type F1 score \uparrow
Random ground-truth	0.197 ± 0.052	0.390 ± 0.136
No fingerprint	0.135 ± 0.046	0.562 ± 0.139
Ours	0.123 ± 0.043	0.627 ± 0.127

of each parameter. These random ground-truth vectors have the same properties as our ground-truth vectors in terms of non-equal distances. But the shuffled feature vectors are meaningless, and are not corresponding to their true model hyperparameters. Due to the randomness nature of this baseline, we perform three random shuffling and then report the averaged performance.

To validate the effects of our proposed fingerprint estimation constraints, we conduct an ablation study and train our framework end-to-end with only the model parsing objective in Eqn. 12. This results in the *no fingerprint* baseline.

Network architecture prediction. We report results of network architecture prediction in Tab. 3 for the 6 testing sets, as defined in Sec. 4.1. Our method achieves a much lower L_1 error compared to the random ground-truth baseline for continuous type parameters and higher F1 score for discrete type parameters. This result indicates that there is indeed a much stronger and generalized correlation between generated images and the embedding space of meaningful architecture hyper-parameters and loss function types, compared to a random vector of the same length and distribution. This correlation is the foundation of why model parsing of GMs can be a valid and solvable research task. Removing fingerprint estimation objectives offers worse results showing the importance of the fingerprint estimation in model parsing.

Figure 6 shows the detailed L_1 error and F1 score for all network architecture parameters. We observe that our method per-

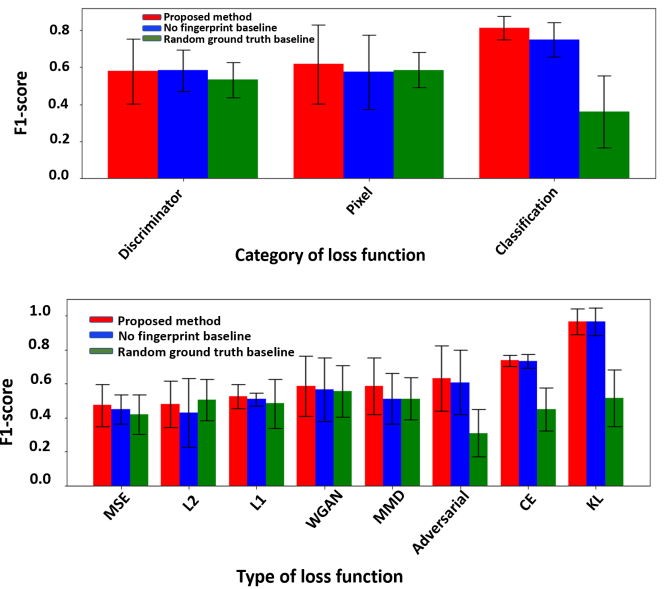


Fig. 7: F1 score for each loss function type at coarse and fine levels averaged across all images of all models in the 6 test sets. We also show the standard deviation of performance across different sets.

TABLE 4: F1 score for coarse-level and fine-level loss type prediction. Our method performs better for both fine-level and coarse-level loss compared to the prediction of each level by itself.

Method	Coarse-level F1 score \uparrow	Fine-level F1 score \uparrow
Random ground-truth	0.492 ± 0.128	0.491 ± 0.136
No fingerprint	0.645 ± 0.135	0.593 ± 0.121
3-D encoding	0.669 ± 0.134	-
8-D encoding	-	0.600 ± 0.125
Ours (hierarchical learning)	0.670 ± 0.131	0.622 ± 0.121

forms substantially better than the random ground-truth baseline for almost all parameters. As for the no fingerprint baseline, our method is still better in most cases with a few parameters showing similar results. We also show the standard deviation of every estimated parameter for all the methods. Our proposed approach in general has smaller standard deviations compared to the two baselines. Even though for some parameters (e.g., # parameters), the performance of random ground-truth is similar, the standard deviation is reducing for our proposed approach showing consistent performance with less variability across different testing sets.

Loss function prediction. To validate the effects of hierarchical learning in the loss function prediction, we ablate with 3-D coarse-level classification and 8-D fine-level classification alone. We calculate the F1 score in both the coarse and fine levels, i.e., 3-D and 8-D classification, respectively. The performance are shown in Tab. 4. For the random ground-truth baseline, the performance is close to a random guess. Hierarchical learning results are comparable to 3-D encoding at the coarse level but better than 8-D encoding at the fine level. These results demonstrate the contribution of our hierarchical learning for loss function prediction.

Figure 7 shows the detailed F1 score for all loss function parameters. Apparently our method works better than both baselines for almost all parameters. We also show the standard deviation of every estimated parameter for all the methods. Similar behaviour of standard deviation for different methods was observed as in the network architecture. Figure 8 provides another perspective of

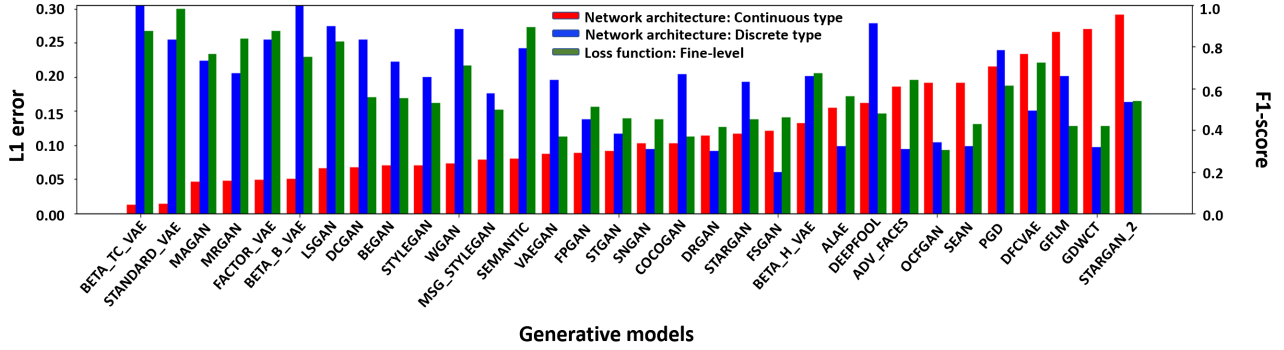


Fig. 8: Performance of all GMs in our 6 testing sets. Similar performance trends are observed for network architecture and loss functions, *i.e.*, if the L_1 error is small for continuous type parameters in network architecture, the high F1 score is also observed for discrete type parameter in network architecture and fine-level loss function. In other words, the abilities to reverse engineer the network architecture and loss functions types for one GM are reasonably consistent.

TABLE 5: Performance comparison by varying the training and testing data for face and non-face GMs. Testing performance on non-face GMs is better compared to face GMs. Training and testing on the same content produces better results than on the different contents.

Test GMs (# GMs)	Train GMs (# GMs)	Network architecture		Loss function	
		Continuous type L_1 error \downarrow	Discrete type F1 score \uparrow	Coarse-level F1 score \uparrow	Fine-level F1 score \uparrow
Face (6)	Face (41)	0.145 \pm 0.051	0.650 \pm 0.110	0.631 \pm 0.151	0.632 \pm 0.130
	Non-face (53)	0.191 \pm 0.060	0.574 \pm 0.115	0.633 \pm 0.100	0.612 \pm 0.100
	Full (94)	0.123 \pm 0.043	0.627 \pm 0.127	0.670 \pm 0.131	0.622 \pm 0.121
Non-face (6)	Non-face (47)	0.115 \pm 0.026	0.775 \pm 0.104	0.537 \pm 0.104	0.672 \pm 0.130
	Face (47)	0.185 \pm 0.032	0.469 \pm 0.089	0.643 \pm 0.114	0.533 \pm 0.117
	Full (94)	0.110 \pm 0.020	0.775 \pm 0.130	0.485 \pm 0.083	0.657 \pm 0.098
Random guess		0.393	0.500	0.500	0.500

TABLE 6: Ablation study of the 4 loss terms in fingerprint estimation. Removing any one loss for fingerprint estimation deteriorates the performance with the worse results in the case of removing all losses.

Loss removed	Network architecture		Loss function	
	Continuous type L_1 error \downarrow	Discrete type F1 score \uparrow	Coarse-level F1 score \uparrow	Fine-level F1 score \uparrow
Magnitude loss	0.127 \pm 0.041	0.604 \pm 0.145	0.661 \pm 0.118	0.609 \pm 0.134
Spectrum loss	0.129 \pm 0.045	0.600 \pm 0.139	0.657 \pm 0.134	0.591 \pm 0.122
Repetitive loss	0.123 \pm 0.045	0.611 \pm 0.140	0.650 \pm 0.115	0.607 \pm 0.111
Energy loss	0.134 \pm 0.039	0.530 \pm 0.152	0.642 \pm 0.144	0.563 \pm 0.132
All (no fingerprint)	0.135 \pm 0.046	0.562 \pm 0.139	0.645 \pm 0.135	0.593 \pm 0.121
Nothing (ours)	0.123 \pm 0.043	0.627 \pm 0.127	0.670 \pm 0.131	0.622 \pm 0.121

model parsing by showing the performance in terms of 27 unique GMs across our 6 testing sets.

4.3 Ablation study

Face vs. non-face GMs. Our dataset consist of 47 GMs trained on face datasets and 53 GMs trained on non-face datasets. In other words, the contents of the images generated by these GMs are quite diverse. Let’s denote these GMs as face GMs and non-face GMs, respectively. All experiments above are conducted by training on 94 GMs and evaluating on 6 face GMs. Here we conduct an ablation study to train and evaluate on different GM types. Similar to the six testing sets for face GMs, we also construct six different testing sets for non-face GMs. Each set consists of two GMs trained on MNIST, two GMs trained on CIFAR10, and two GMs trained on other datasets. We study the performance on these face and non-face testing sets when training on three different training sets, including only face GMs, only non-face GMs and all GMs. Note that all testing GMs are excluded during training each time and the performance are averaged across

all testing sets. We also add a baseline where both regression and classification make a random guess on their estimation.

The results are shown in Tab. 5. We have three observations. First, model parsing for non-face GMs are easier than face GMs. This might be partially due to the generally lower-quality images generated by non-face GMs compared to those by face GMs, thus more traces are remained for model parsing. Second, training and testing on the same content can generate better results than on different contents. Third, training on the full datasets improves some parameter estimation but may hurt other parameters slightly.

Weighted cross-entropy loss. As mentioned before, the ground truth of many network hyperparameters have biased distributions. For example, the “normalization type” parameter in Tab. 1 has uneven distribution among its 4 possible types. With this biased distribution, our classifier might make a constant prediction to the type with the highest probability in the ground truth, as this could minimize the loss especially for severe biasness. This degenerate classifier clearly has no value to model parsing. To address this issue, we propose to use the weighted cross-entropy loss with

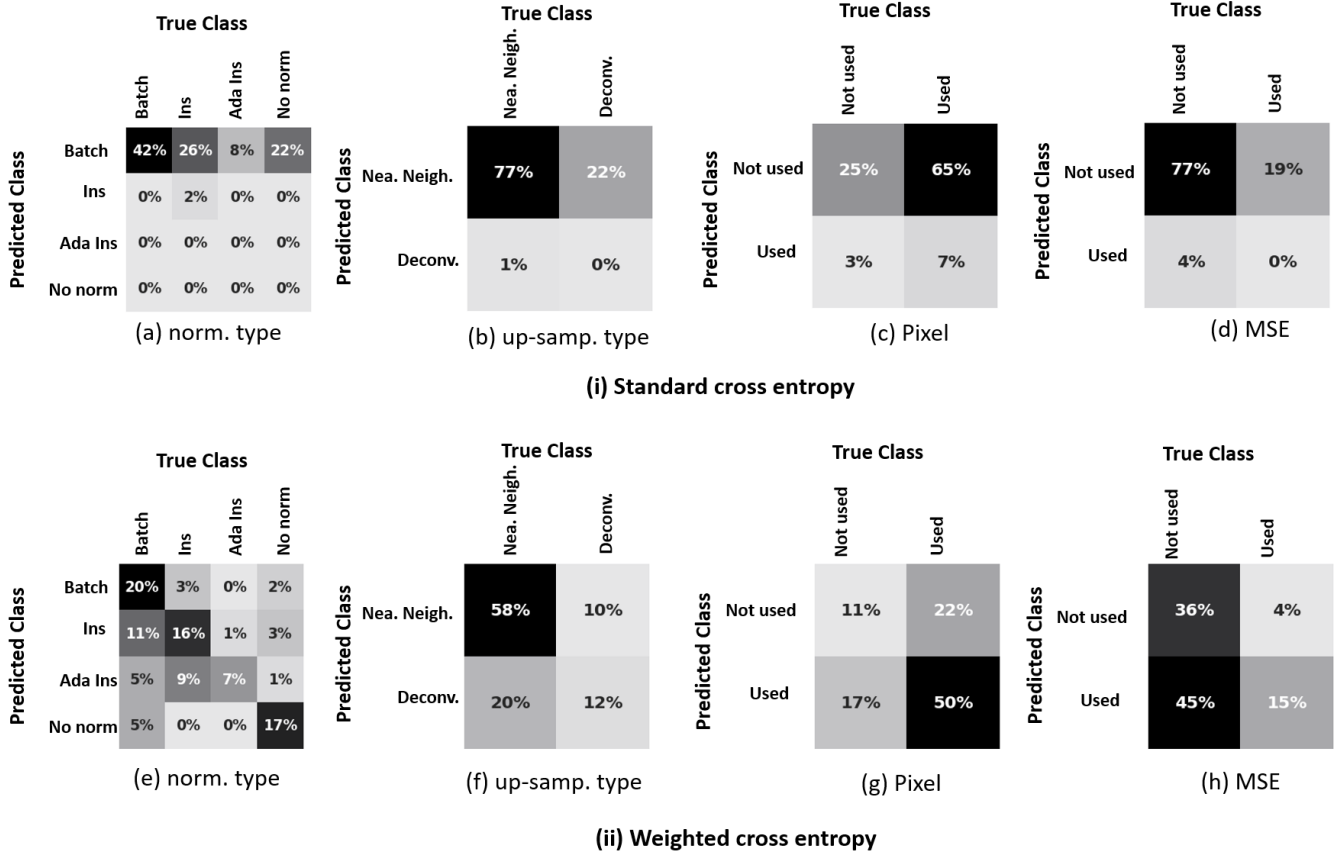


Fig. 9: Confusion matrix in the estimation of four parameters in the network architecture and loss function. (a)-(d): Standard cross-entropy and (e)-(f): Weighted cross entropy. Weighted cross entropy handles imbalance of data much better than the standard cross entropy which usually predicts one class.

TABLE 7: Network architecture estimation and loss function prediction when given multiple images of one GM. Performance increases when increasing number of images for evaluation from 1 to 10. Performance becomes stable for more than 10 images.

# images	Network architecture		Loss function	
	Continuous type L_1 error \downarrow	Discrete type F1 score \uparrow	Coarse-level F1 score \uparrow	Fine-level F1 score \uparrow
1	0.122 \pm 0.043	0.631 \pm 0.121	0.671 \pm 0.130	0.620 \pm 0.112
10	0.109 \pm 0.046	0.668 \pm 0.140	0.706 \pm 0.161	0.654 \pm 0.140
100	0.108 \pm 0.047	0.685 \pm 0.144	0.706 \pm 0.172	0.646 \pm 0.158
500	0.108 \pm 0.046	0.686 \pm 0.143	0.699 \pm 0.170	0.644 \pm 0.164

different loss weight for each class. These weights are calculated using the ground-truth distribution of every parameter in the full dataset. To validate if the above approach is able to remedy this issue, we compare it with the standard cross-entropy loss.

Figure 9 shows the confusion matrix for discrete type parameters in network architecture prediction and coarse/fine level parameters in loss function prediction. The rows in the confusion matrix are represented by predicted classes and columns are represented by the ground-truth classes. We clearly see that the classifier is mostly biased towards more frequent classes in all 4 examples, when the standard cross-entropy loss is used. However, this problem is remedied when using the weighted cross-entropy loss, and the classifiers make meaningful predictions.

Fingerprint losses. We proposed four loss terms in Sec. 3.2 to guide the training of the fingerprint estimation including magnitude loss, spectrum loss, repetitive loss and energy loss. We conduct an ablation study to demonstrate the importance of these four losses in our proposed method. Therefore, we perform four experiments, each time removing one of the loss terms and

compare the performance with our proposed method (remove nothing) and no fingerprint baseline (remove all). As shown in Tab. 6, removing any loss for fingerprint estimation hurts the performance. Our “no fingerprint” baseline, for which we remove all losses performs worst of all. Therefore, each loss clearly has a positive effect on the fingerprint estimation and model parsing of hyperparameters.

Model parsing with multiple images. We evaluate model parsing when varying the number of test images. For each GM, we randomly select 1, 10, 100, and 500 images per GM from different face GMs sets for evaluation. With multiple images per GM, we average the prediction for continuous type parameters and take majority voting for discrete type parameters and loss function parameters. We compute the L_1 error and F1 score for the continuous and discrete type parameters respectively and average the result across different sets. We repeat the above experiment multiple times, each time randomly selecting the number of images. We compare the L_1 error and F1 score for respective parameters. Tab. 7 shows noticeable gains with 10 images and

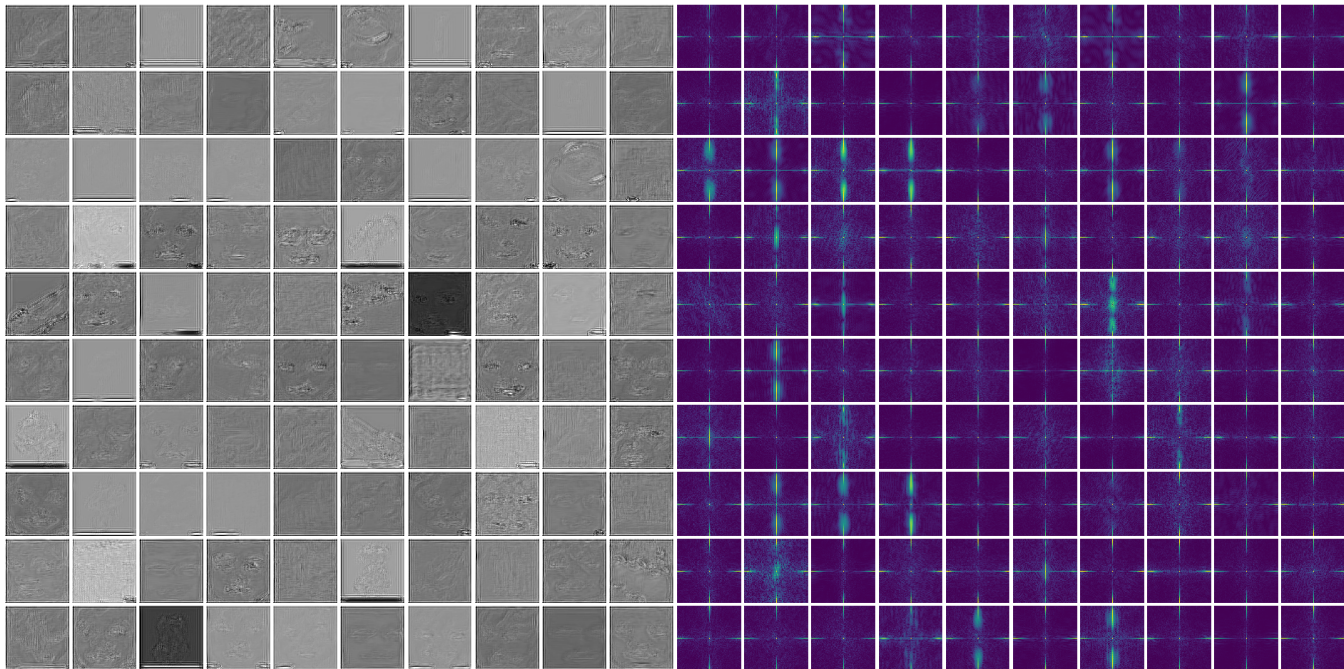


Fig. 10: Estimated fingerprints (left) and corresponding frequency spectrum (right) from one generated image of each of 100 GMs. Many frequency spectrums show distinct high frequency signals, while some appear to be similar to each other.

minor gains with 100 images. There is no much performance difference when evaluating on 100 or 500 images, which suggests that our framework is robust in generating consistent results when tested on different numbers of generated images by the same GM.

Content-independent fingerprint. Ideally our estimated fingerprint should be independent of the content of the image. That is, the fingerprint only includes the trace left by the GM while not indicating the content in any way. To validate this, we partition all GMs into four classes based on their contents: FACES (47 GMs), MNIST (14), CIFAR10 (28), and OTHER (11). Every class has images generated by the GMs belong to this class. We feed these images to a pre-trained FEN and obtain their fingerprints. Then we train a shallow network consisting of five convolutional layers and two fully connected layers for a 4-way classification. However, we observe the training cannot converge. This means that our estimated fingerprint from FEN doesn't have any content specific properties for content classification. As a result, the model parsing of the hyperparameters doesn't leverage the content information across different GMs, which is a desirable property.

4.4 Visualization

Figure 10 shows an estimated fingerprint image and its frequency spectrum for a randomly selected image per GM. We observe that estimated fingerprints have the desired properties defined by our loss terms, including low magnitude and highlights in middle and high frequencies.

We also find that the fingerprints estimated from different generated images of the same GM are similar. To quantify this, we compute a Cosine similarity matrix $\mathbf{C} \in \mathbb{R}^{100 \times 100}$ where $\mathbf{C}(i, j)$ is the averaged Cosine similarity of 50 randomly sampled fingerprint pairs from GM i and j . The matrix \mathbf{C} in Figure 11 clearly illustrates the higher intra-GM and lower inter-GM fingerprint similarities.

TABLE 8: AUC for deepfake detection on the Celeb-DF dataset [29].

Method	Training Data	AUC (%)
Methods training with <i>pixel-level</i> supervision		
Xception+Reg [14]	DFFD	64.4
Xception+Reg [14]	DFFD, UADFV	71.2
Methods training with <i>image-level</i> supervision		
Two-stream [52]	Private	53.8
Meso4 [53]		54.8
VA-LogReg [54]		55.1
DSP-FWA [55]		64.6
Multi-task [56]	FF	54.3
Capsule [57]	FF++	57.5
Xception-c40 [10]		65.5
HeadPose [58]	UADFV	54.6
FWA [59]		56.9
Xception [14]		52.2
Xception+Reg [14]		57.1
Ours		64.7
Xception [14]	DFFD	63.9
Ours		65.3
Xception [14]	DFFD, UADFV	67.6
Ours		70.2

TABLE 9: Classification rates of image attribution. The baseline results are cited from [16].

Method	CelebA	LSUN
kNN	28.00	36.30
Eigenface [60]	53.28	-
PRNU [28]	86.61	67.84
Zhuet <i>al.</i> [16]	99.43	98.58
Ours	99.66	99.84

4.5 Deepfake detection and image attribution

Deepfake detection Our FEN can be adopted for deepfake detection by adding a shallow network for binary classification. We evaluate our method on the recently introduced Celeb-DF dataset [29]. We experiment with two training sets, UADFV and DFFD, in order to compare with previous results. We follow the

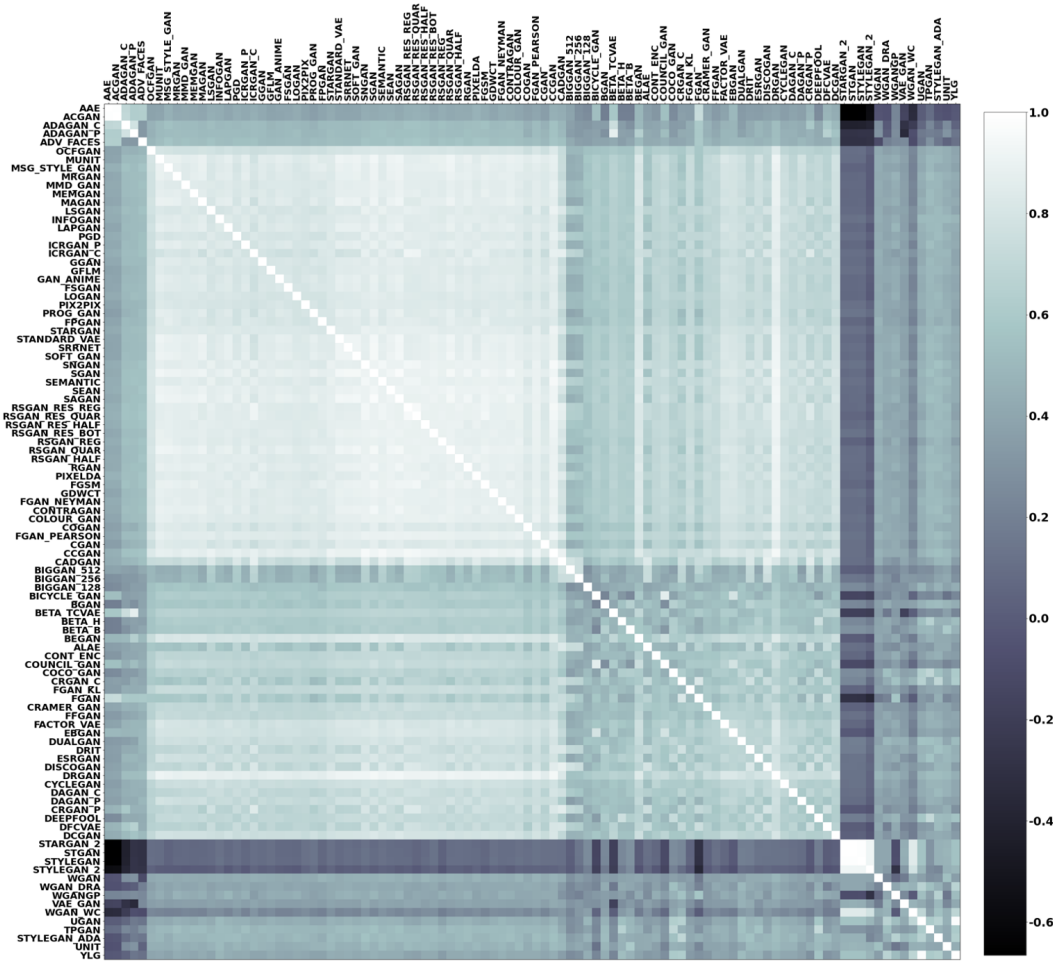


Fig. 11: Cosine similarity matrix for pairs of 100 GM’s fingerprints. Each element of this matrix is the average Cosine similarities of 50 pairs of fingerprints from two GMs. We see the higher intra-GM and lower inter-GM similarities. Also, two clusters of GMs are similar within their respective cluster. One includes 4 GMs: StarGAN-2, StGAN, StyleGAN, and StyleGAN-2. And the other is a larger cluster includes different versions of RSGAN, BIGGAN, etc., which have either very similar network architectures or loss functions.

same training protocols used in [14] for UADFV and DFFD.

We report the Area Under Curve (AUC) in Tab. 8. Compared with methods trained on UADFV, our approach achieves a significantly better result, despite the more advanced backbones used by others. Our results when trained on DFFD and UADFV fall only slightly behind the best score reported by Xception+Reg [14]. Importantly, however, they trained with pixel-level supervision which are typically unavailable. These results are provided for completeness, but are not directly comparable to all other methods trained with only image-level supervision for binary classification. Compared to all other methods, our method provides the highest deepfake detection AUC.

Image attribution. Similar to deepfake detection, we use a shallow network for image attribution. The only difference is that image attribution is a multi-class task and depends on the number of GMs during training. Following [16], we train our model on 100K genuine and 100K fake face images each from four GMs: SNGAN [61], MMDGAN [62], CRAMERGAN [63] and ProGAN [4], for five-class classification. Tab. 9 reports the performance. Our result on CelebA [29] and LSUN [49] outperform the performance in [16]. This again validates the generalization ability of the proposed fingerprint estimation.

5 CONCLUSION

In this paper, we define the model parsing problem as inferring the network architectures and training loss functions of a GM from the generative images. We make the first attempt to tackle this challenge problem. The main idea is to estimate the fingerprint for each image and use it for model parsing. Four constraints are developed for fingerprint estimation. Our framework can not only perform model parsing, but also extend to deepfake detection and image attribution. We have collected a large-scale fake image dataset from 100 different GMs. Various experiments have validated the effects of different components in our approach.

ACKNOWLEDGEMENT

This work was partially supported by Facebook AI. This material, except Section 4.5 and related efforts, is based upon work partially supported by the Defense Advanced Research Projects Agency (DARPA) under Agreement No. HR00112090131 to Xiaoming Liu at Michigan State University.

REFERENCES

[1] I. Goodfellow, J. Pouget-Abadie, M. Mirza, B. Xu, D. Warde-Farley, S. Ozair, A. Courville, and Y. Bengio, “Generative adversarial nets,” in *NeurIPS*, 2014.

- [2] T. Karras, S. Laine, and T. Aila, "A style-based generator architecture for generative adversarial networks," in *CVPR*, 2019.
- [3] Y. Choi, M. Choi, M. Kim, J.-W. Ha, S. Kim, and J. Choo, "StarGAN: Unified generative adversarial networks for multi-domain image-to-image translation," in *CVPR*, 2018.
- [4] T. Karras, T. Aila, S. Laine, and J. Lehtinen, "Progressive growing of GANs for improved quality, stability, and variation," in *ICLR*, 2018.
- [5] D. P. Kingma and M. Welling, "Auto-encoding variational bayes," in *ICLR*, 2014.
- [6] C. P. Burgess, I. Higgins, A. Pal, L. Matthey, N. Watters, G. Desjardins, and A. Lerchner, "Understanding disentangling in β -VAE," in *NeurIPS*, 2017.
- [7] R. T. Q. Chen, X. Li, R. Grosse, and D. Duvenaud, "Isolating sources of disentanglement in variational autoencoders," in *NeurIPS*, 2018.
- [8] C. Waldemarsson, *Disinformation, Deepfakes & Democracy: The European response to election interference in the digital age*. The Alliance of Democracies Foundation, 2020.
- [9] V. Heath, "From a sleazy Reddit post to a national security threat: A closer look at the deepfake discourse," in *Disinformation and Digital Democracies in the 21st Century*. The NATO Association of Canada, 2019.
- [10] A. Rossler, D. Cozzolino, L. Verdoliva, C. Riess, J. Thies, and M. Nießner, "FaceForensics++: Learning to detect manipulated facial images," in *ICCV*, 2019.
- [11] S. McCloskey and M. Albright, "Detecting GAN-generated imagery using saturation cues," in *ICIP*, 2019.
- [12] L. Guarnera, O. Giudice, and S. Battiato, "Deepfake detection by analyzing convolutional traces," in *CVPRW*, 2020.
- [13] F. Marra, C. Saltori, G. Boato, and L. Verdoliva, "Incremental learning for the detection and classification of GAN-generated images," in *WIFS*, 2019.
- [14] H. Dang, F. Liu, J. Stehouwer, X. Liu, and A. K. Jain, "On the detection of digital face manipulation," in *CVPR*, 2020.
- [15] Y. Nirkin, L. Wolf, Y. Keller, and T. Hassner, "Deepfake detection based on the discrepancy between the face and its context," *arXiv preprint arXiv:2008.12262*, 2020.
- [16] N. Yu, L. S. Davis, and M. Fritz, "Attributing fake images to GANs: Learning and analyzing GAN fingerprints," in *ICCV*, 2019.
- [17] F. Tramèr, F. Zhang, A. Juels, M. K. Reiter, and T. Ristenpart, "Stealing machine learning models via prediction APIs," in *USENIXSS*, 2016.
- [18] S. J. Oh, M. Augustin, M. Fritz, and B. Schiele, "Towards reverse-engineering black-box neural networks," in *ICLR*, 2018.
- [19] W. Hua, Z. Zhang, and G. E. Suh, "Reverse engineering convolutional neural networks through side-channel information leaks," in *DAC*, 2018.
- [20] L. Batina, S. Bhasin, D. Jap, and S. Picek, "CSI NN: Reverse engineering of neural network architectures through electromagnetic side channel," in *USENIXSS*, 2019.
- [21] J. Lukas, J. Fridrich, and M. Goljan, "Digital camera identification from sensor pattern noise," *IEEE Transactions on Information Forensics and Security*, vol. 1, no. 2, pp. 205–214, 2006.
- [22] M. Goljan, J. Fridrich, and T. Filler, "Large scale test of sensor fingerprint camera identification," *Media forensics and security*, vol. 7254, p. 72540I, 2009.
- [23] K. Kurosawa, K. Kuroki, and N. Saitoh, "CCD fingerprint method-identification of a video camera from videotaped images," in *ICIP*, 1999.
- [24] T. Filler, J. Fridrich, and M. Goljan, "Using sensor pattern noise for camera model identification," in *ICIP*, 2008.
- [25] D. Valsesia, G. Coluccia, T. Bianchi, and E. Magli, "Compressed fingerprint matching and camera identification via random projections," *IEEE Transactions on Information Forensics and Security*, vol. 10, no. 7, pp. 1472–1485, 2015.
- [26] J. Lukáš, J. Fridrich, and M. Goljan, "Detecting digital image forgeries using sensor pattern noise," *Security, Steganography, and Watermarking of Multimedia Contents VIII*, vol. 6072, p. 60720Y, 2006.
- [27] M. Chen, J. Fridrich, M. Goljan, and J. Lukáš, "Determining image origin and integrity using sensor noise," *IEEE Transactions on Information Forensics and Security*, vol. 3, no. 1, pp. 74–90, 2008.
- [28] F. Marra, D. Gragnaniello, L. Verdoliva, and G. Poggi, "Do GANs leave artificial fingerprints?" in *MIPR*, 2019.
- [29] Y. Li, X. Yang, P. Sun, H. Qi, and S. Lyu, "Celeb-DF: A large-scale challenging dataset for deepfake forensics," in *CVPR*, 2020.
- [30] D. Cozzolino and L. Verdoliva, "Noiseprint: a CNN-based camera model fingerprint," *IEEE Transactions on Information Forensics and Security*, vol. 15, pp. 144–159, 2019.
- [31] S.-Y. Wang, O. Wang, R. Zhang, A. Owens, and A. A. Efros, "CNN-generated images are surprisingly easy to spot... for now," in *CVPR*, 2020.
- [32] X. Zhang, S. Karaman, and S.-F. Chang, "Detecting and simulating artifacts in GAN fake images," in *WIFS*, 2019.
- [33] T. K. Moon, "The expectation-maximization algorithm," *Signal processing magazine*, vol. 13, no. 6, pp. 47–60, 1996.
- [34] L. Chai, D. Bau, S.-N. Lim, and P. Isola, "What makes fake images detectable? Understanding properties that generalize," in *ECCV*, 2020.
- [35] A. Vaswani, N. Shazeer, N. Parmar, J. Uszkoreit, L. Jones, A. N. Gomez, L. Kaiser, and I. Polosukhin, "Attention is all you need," in *NeurIPS*, 2017.
- [36] Y. Nirkin, I. Masi, A. T. Tuan, T. Hassner, and G. Medioni, "On face segmentation, face swapping, and face perception," in *FGR*. IEEE, 2018, pp. 98–105.
- [37] Z. Wang, Q. She, and T. E. Ward, "Generative adversarial networks in computer vision: A survey and taxonomy," *ACM Computing Surveys*, vol. 54, no. 2, 2021.
- [38] A. Jabbar, X. Li, and B. Omar, "A survey on generative adversarial networks: Variants, applications, and training," *arXiv preprint arXiv:2006.05132*, 2020.
- [39] Z. Liu, P. Luo, X. Wang, and X. Tang, "Deep learning face attributes in the wild," in *ICCV*, 2015.
- [40] L. Deng, "The MNIST database of handwritten digit images for machine learning research [best of the web]," *Signal Processing Magazine*, vol. 29, no. 6, pp. 141–142, 2012.
- [41] A. Krizhevsky, G. Hinton *et al.*, "Learning multiple layers of features from tiny images," 2009.
- [42] J. Deng, W. Dong, R. Socher, L.-J. Li, K. Li, and L. Fei-Fei, "ImageNet: A large-scale hierarchical image database," in *CVPR*, 2009.
- [43] J.-Y. Zhu, T. Park, P. Isola, and A. A. Efros, "Unpaired image-to-image translation using cycle-consistent adversarial networks," in *ICCV*, 2017.
- [44] K. Zhang, W. Zuo, Y. Chen, D. Meng, and L. Zhang, "Beyond a gaussian denoiser: Residual learning of deep CNN for image denoising," *IEEE Transactions on Image Processing*, vol. 26, no. 7, pp. 3142–3155, 2017.
- [45] A. Jourabloo, Y. Liu, and X. Liu, "Face de-spoofing: Anti-spoofing via noise modeling," in *ECCV*, 2018.
- [46] M. Tan, B. Chen, R. Pang, V. Vasudevan, M. Sandler, A. Howard, and Q. V. Le, "MnasNet: Platform-aware neural architecture search for mobile," in *CVPR*, 2019.
- [47] H. Pham, M. Guan, B. Zoph, Q. Le, and J. Dean, "Efficient neural architecture search via parameters sharing," in *ICML*, 2018.
- [48] C. Liu, B. Zoph, M. Neumann, J. Shlens, W. Hua, L.-J. Li, L. Fei-Fei, A. Yuille, J. Huang, and K. Murphy, "Progressive neural architecture search," in *ECCV*, 2018.
- [49] F. Yu, Y. Zhang, S. Song, A. Seff, and J. Xiao, "LSUN: Construction of a large-scale image dataset using deep learning with humans in the loop," *arXiv preprint arXiv:1506.03365*, 2015.
- [50] G. Forman and M. Scholz, "Apples-to-apples in cross-validation studies: pitfalls in classifier performance measurement," *Association for Computing Machinery SIGKDD Explorations Newsletter*, vol. 12, no. 1, pp. 49–57, 2010.
- [51] L. A. Jeni, J. F. Cohn, and F. De La Torre, "Facing imbalanced data-recommendations for the use of performance metrics," in *ACII*, 2013.
- [52] X. Han, V. Morariu, P. I. Larry Davis *et al.*, "Two-stream neural networks for tampered face detection," in *CVPRW*, 2017.
- [53] D. Afchar, V. Nozick, J. Yamagishi, and I. Echizen, "MesoNet: a compact facial video forgery detection network," in *WIFS*, 2018.
- [54] F. Matern, C. Riess, and M. Stamminger, "Exploiting visual artifacts to expose deepfakes and face manipulations," in *WACVW*, 2019.
- [55] K. He, X. Zhang, S. Ren, and J. Sun, "Spatial pyramid pooling in deep convolutional networks for visual recognition," *IEEE Transactions on Pattern Analysis and Machine Intelligence*, vol. 37, no. 9, pp. 1904–1916, 2015.
- [56] H. H. Nguyen, F. Fang, J. Yamagishi, and I. Echizen, "Multi-task learning for detecting and segmenting manipulated facial images and videos," in *BTAS*, 2019.
- [57] H. H. Nguyen, J. Yamagishi, and I. Echizen, "Capsule-forensics: Using capsule networks to detect forged images and videos," in *ICASSP*, 2019.
- [58] X. Yang, Y. Li, and S. Lyu, "Exposing deep fakes using inconsistent head poses," in *ICASSP*, 2019.
- [59] Y. Li and S. Lyu, "Exposing DeepFake videos by detecting face warping artifacts," in *CVPRW*, 2019.
- [60] L. Sirovich and M. Kirby, "Low-dimensional procedure for the characterization of human faces," *Journal of the Optical Society of America*, vol. 4, no. 3, pp. 519–524, 1987.
- [61] T. Miyato, T. Kataoka, M. Koyama, and Y. Yoshida, "Spectral normalization for generative adversarial networks," in *ICLR*, 2018.

- [62] C.-L. Li, W.-C. Chang, Y. Cheng, Y. Yang, and B. Póczos, "MMD GAN: Towards deeper understanding of moment matching network," in *NeurIPS*, 2017.
- [63] M. G. Bellemare, I. Danihelka, W. Dabney, S. Mohamed, B. Lakshminarayanan, S. Hoyer, and R. Munos, "The cramer distance as a solution to biased wasserstein gradients," *arXiv preprint arXiv:1705.10743*, 2017.
- [64] G. Ateniese, L. V. Mancini, A. Spognardi, A. Villani, D. Vitali, and G. Felici, "Hacking smart machines with smarter ones: How to extract meaningful data from machine learning classifiers," *International Journal of Security and Networks*, vol. 10, no. 3, pp. 137–150, 2015.
- [65] R. Shokri, M. Stronati, C. Song, and V. Shmatikov, "Membership inference attacks against machine learning models," in *SP*, 2017.
- [66] B. Škrlj, S. Džeroski, N. Lavrač, and M. Petkovič, "Feature importance estimation with self-attention networks," in *ECAI*, 2019.
- [67] G. Chierchia, G. Poggi, C. Sansone, and L. Verdoliva, "A bayesian-MRF approach for PRNU-based image forgery detection," *IEEE Transactions on Information Forensics and Security*, vol. 9, no. 4, pp. 554–567, 2014.
- [68] D. Cozzolino, D. Gragnaniello, and L. Verdoliva, "Image forgery localization through the fusion of camera-based, feature-based and pixel-based techniques," in *ICIP*, 2014.
- [69] S. Chakraborty and M. Kirchner, "PRNU-based image manipulation localization with discriminative random fields," *Electronic Imaging*, vol. 2017, no. 7, pp. 113–120, 2017.
- [70] P. Korus and J. Huang, "Multi-scale analysis strategies in PRNU-based tampering localization," *IEEE Transactions on Information Forensics and Security*, vol. 12, no. 4, pp. 809–824, 2016.
- [71] D. Berthelot, T. Schumm, and L. Metz, "BEGAN: Boundary equilibrium generative adversarial networks," *arXiv preprint arXiv:1703.10717*, 2017.
- [72] H. Kim and A. Mnih, "Disentangling by factorising," in *ICML*, 2018.
- [73] I. Higgins, L. Matthey, A. Pal, C. Burgess, X. Glorot, M. Botvinick, S. Mohamed, and A. Lerchner, " β -VAE: Learning basic visual concepts with a constrained variational framework," in *ICLR*, 2017.
- [74] C. H. Lin, C.-C. Chang, Y.-S. Chen, D.-C. Juan, W. Wei, and H.-T. Chen, "COCO-GAN: generation by parts via conditional coordinating," in *ICCV*, 2019.
- [75] Y. Yu, Z. Gong, P. Zhong, and J. Shan, "Unsupervised representation learning with deep convolutional neural network for remote sensing images," in *ICIG*, 2017.
- [76] X. Hou, L. Shen, K. Sun, and G. Qiu, "Deep feature consistent variational autoencoder," in *WACV*, 2017.
- [77] L. Tran, X. Yin, and X. Liu, "Disentangled representation learning GAN for pose-invariant face recognition," in *CVPR*, 2017.
- [78] X. Yin, X. Yu, K. Sohn, X. Liu, and M. Chandraker, "Towards large-pose face frontalization in the wild," in *ICCV*, 2017.
- [79] Y. Nirkin, Y. Keller, and T. Hassner, "FSGAN: Subject agnostic face swapping and reenactment," in *ICCV*, 2019.
- [80] R. Wang, A. Cully, H. J. Chang, and Y. Demiris, "MAGAN: Margin adaptation for generative adversarial networks," *arXiv preprint arXiv:1704.03817*, 2017.
- [81] T. Che, Y. Li, A. P. Jacob, Y. Bengio, and W. Li, "Mode regularized generative adversarial networks," in *ICLR*, 2017.
- [82] A. F. Ansari, J. Scarlett, and H. Soh, "A characteristic function approach to deep implicit generative modeling," in *CVPR*, 2020.
- [83] H. Zhang, I. Goodfellow, D. Metaxas, and A. Odena, "Self-attention generative adversarial networks," in *ICML*, 2019.
- [84] P. Zhu, R. Abdal, Y. Qin, and P. Wonka, "SEAN: Image synthesis with semantic region-adaptive normalization," in *CVPR*, 2020.
- [85] Y. Choi, Y. Uh, J. Yoo, and J.-W. Ha, "StarGAN v2: Diverse image synthesis for multiple domains," in *CVPR*, 2020.
- [86] M. Liu, Y. Ding, M. Xia, X. Liu, E. Ding, W. Zuo, and S. Wen, "STGAN: A unified selective transfer network for arbitrary image attribute editing," in *CVPR*, 2019.
- [87] T. Karras, S. Laine, M. Aittala, J. Hellsten, J. Lehtinen, and T. Aila, "Analyzing and improving the image quality of StyleGAN," in *CVPR*, 2020.
- [88] R. Huang, S. Zhang, T. Li, and R. He, "Beyond face rotation: Global and local perception GAN for photorealistic and identity preserving frontal view synthesis," in *ICCV*, 2017.
- [89] A. B. L. Larsen, S. K. Sønderby, H. Larochelle, and O. Winther, "Autoencoding beyond pixels using a learned similarity metric," in *ICML*, 2016.
- [90] C. Chen, Z. Xiong, X. Liu, and F. Wu, "Camera trace erasing," in *CVPR*, 2020.



Vishal Asnani is pursuing his Ph. D. degree in the Computer Science and Engineering department from Michigan State University since 2021. He received his Bachelor's degree in Electrical and Instrumentation Engineering from Birla Institute of technology and Science, Pilani, India in 2019. His research interests include computer vision and machine learning with a focus on the studying of generative models and deepfake detection.



Xi Yin is a Research Scientist at Facebook AI Applied Research team. She received her Ph.D. degree in Computer Science and Engineering from Michigan State University in 2018. Before joining Facebook AI, she was an Senior Applied Scientist at Microsoft Cloud and AI. Her research is focused on computer vision, deep learning, vision and language. She has co-authored 18 papers in top vision conferences and journals, and filed 3 U.S. patents. She has received Best Student Paper Award at WACV 2014. She is an Area Chair for IJCB 2021 and ICCV 2021.



Tal Hassner Tal Hassner received his M.Sc. and Ph.D. degrees in applied mathematics and computer science from the Weizmann Institute of Science in 2002 and 2006, respectively. In 2008 he joined the Department of Math. and Computer Science at The Open Univ. of Israel where he was an Associate Professor until 2018. From 2015 to 2018, he was a senior computer scientist at the Information Sciences Institute (ISI) and a Visiting Research Associate Professor at the Institute for Robotics and Intelligent Systems, Viterbi School of Engineering, both at USC, CA, USA. From 2018 to 2019, he was a principal applied scientist at AWS Rekognition. Since 2019 he is an applied research lead at Facebook AI, supporting both the text and people photo understanding teams. He has been a program chair at WACV'18 and ICCV'21, workshop chair at CVPR'20, tutorial chair at ICCV'17 and ECCV'22, and area chair in CVPR, ECCV, AAAI, and others. Finally, he is an associate editor at IEEE TPAMI and TBIOM.



Xiaoming Liu is a MSU Foundation Professor at the Department of Computer Science and Engineering of Michigan State University. He received the Ph.D. degree in Electrical and Computer Engineering from Carnegie Mellon University in 2004. Before joining MSU in Fall 2012, he was a research scientist at General Electric (GE) Global Research. His research interests include computer vision, machine learning, and biometrics. As a co-author, he is a recipient of Best Industry Related Paper Award runner-up at ICPR 2014, Best Student Paper Award at WACV 2012 and 2014, Best Poster Award at BMVC 2015, and Michigan State University College of Engineering Withrow Endowed Distinguished Scholar Award. He has been the Area Chair for numerous conferences, including CVPR, ICCV, ECCV, ICLR, NeurIPS, the Program CO-Chair of WACV'18, BTAS'18, AVSS'22 conferences, and General Co-Chair of FG'23 conference. He is an Associate Editor of Pattern Recognition Letters, Pattern Recognition, and IEEE Transactions on Image Processing. He has authored more than 150 scientific publications, and has filed 29 U.S. patents. He is a fellow of IAPR.

Reverse Engineering of Generative Models: Inferring Model Hyperparameters from Generated Images – Supplementary material –

Vishal Asnani, Xi Yin, Tal Hassner, Xiaoming Liu



1 TEST SETS FOR EVALUATION

The experiments described in the text were performed on two different types of data: face and non-face. Both type of data has six different test sets, each set containing six different GMs for the leave out testing. For face test sets, we follow the distribution of GMs as follows: three GANs, two VAEs and one AA model. We select this distribution because of the number of GMs of each type in our dataset which has 81 GANs, 13 VAEs and 6 AAs. The sets considered are shown in Table 1.

For non-face test sets, we don't have AAs corresponding to non-face data in our dataset. Therefore, considering the above fact and the variability of different types of data, we follow the distribution of GMs as follows: two GMs trained on MNIST data, two GMs trained on CIFAR10 data and last two were randomly selected from the remaining GMs trained on non-face data. The sets considered are shown in Table 2.

2 GROUND TRUTH FOR GMS

We collected a fake face dataset of 100 GMs, each of them with 1,000 generated images. We also collect the ground truth hyperparameters for network architecture and loss function types. Table 3 shows the ground truth representation of the network architecture where different hyperparameters are of different data types. Therefore, we apply min-max normalization for the continuous type parameters to make all values in the range of $[0, 1]$. For multi-class and binary labels, we further show the feature value for different labels in Table 5. Note that some parameters share the same values but with different meanings. For example, F14 and F15 represent skip connection and down-sampling respectively. Table 6 shows the ground truth representation of the loss function types used to train each GM where all these values are binary indicating whether the particular loss type was used or not.

3 NETWORK ARCHITECTURE

Figure 5 shows the network architecture used in different experiments. For GM parsing, our FEN has two stem convolution layers and 15 convolution blocks with each block having convolution, batch normalization and ReLU activation to estimate the fingerprint. The encoder in the PN has five convolution blocks with each

block having convolution, pooling and ReLU activation. This is followed by two fully connected layers to output a 512 dimension feature vector which is further given as input to multiple branches to output different predictions. For continuous type parameters, we use two fully connected layers to output a 9-D network architecture. For discrete type parameters and loss function parameters, we use separate classifiers with three fully connected layers for every parameter to perform multi-class or binary classification.

For the deepfake detection task, we change the architecture of our FEN network as current deepfake manipulation detection requires much deeper networks. Thus, our FEN architecture has two stem convolution layers and 29 convolution blocks to estimate the fingerprint. For further classification, we use a shallow network of five convolution blocks followed by two fully connected layers.

For the image attribution task, we use the same FEN as used in model parsing, and a shallow network of two convolution blocks and two fully connected layers to perform multi-class classification.

4 FEATURE HEATMAPS

Every hyperparameter defined for network architecture and loss function type prediction may depend on certain region of the input image. To find out which region of the input image our model is looking at to predict each hyperparameter, we mask out 5×5 region from the input image. For the continuous type parameters, we compute the L_1 error between every predicted hyperparameter and its ground truth. This value of error will tell us how important is this 5 region in the input image to predict a particular hyperparameter. The higher the value of this error, the higher is the importance of that region in the prediction of the corresponding hyperparameter. For discrete type parameters in network architecture and loss function, we estimate the probability of the ground truth label for every parameter. We subtract this probability from one to estimate the heatmap of the respective feature. Important regions will not affect the probability of the ground truth label for a particular feature. To obtain a stable heatmap, we do the above experiment on 100 randomly chosen images across the different GMs and then calculate the average heatmap.

TABLE 1: Test sets for face data. Each set contains three GANs, two VAEs and one AA.

Set	GM 1	GM 2	GM 3	GM 4	GM 5	GM 6
Set 1	ADV_FACES	BEGAN	BETA_B	BETA_H	DCGAN	FPGAN
Set 2	BETA_H	BETA_TCVAE	DEEFOOL	DRGAN	FSGAN	LSGAN
Set 3	GFLM	MRGAN	MSG_STYLE_GAN	OCFGAN	SEAN	VAE_GAN
Set 4	DFCVAE	FPGAN	MAGAN	PGD	STANDARD_VAE	STARGAN_2
Set 5	ALAE	BETA_B	SEMANTIC	SNGAN	STARGAN	STGAN
Set 6	COCO_GAN	DFCVAE	FACTOR_VAE	GDWCT	STYLEGAN	WGAN

TABLE 2: Test sets for non-face data. Each set contains two GMs from MNIST data, two GMs from CIFAR10 data and 2 GMs from other data.

Set	GM 1	GM 2	GM 3	GM 4	GM 5	GM 6
Set 1	BGAN	CADGAN	CYCLEGAN	GGAN	WGAN_WC	YLG
Set 2	BIGGAN_128	FGAN	CGAN	CONTRAGAN	DISCOGAN	WGAN_DRA
Set 3	AAE	BIGGAN_256	COGAN	CRGAN_P	DUALGAN	ICRGAN_P
Set 4	BIGGAN_512	CRGAN_C	EBGAN	ICRGAN_C	INFOGAN	MUNIT
Set 5	ADAGAN_P	BICYCLE_GAN	DAGAN_P	PEXELDA	RGAN	UNIT
Set 6	ADAGAN_C	DAGAN_C	DRIT	PIX2PIX	SGAN	SOFT_GAN

Figure 1, 2 and 3 show the feature heatmaps for every hyperparameter of network architecture and loss type feature vector for Face, MNIST and CIFAR data respectively. For each hyperparameter, there are certain regions of the input that are more important than others. Each type of data has different type of heatmaps indicating different regions of importance. For face and CIFAR, these regions lie mostly in the central part but for MNIST, many of the features depend on the regions closer to edges. There are also some similarities between these heatmaps for a particular type of data. This can indicate the similarity of these hyperparameters.

REFERENCES

- [1] A. Makhzani, J. Shlens, N. Jaitly, I. Goodfellow, and B. Frey, "Adversarial autoencoders," in *ICLR*, 2016.
- [2] A. Odena, C. Olah, and J. Shlens, "Conditional image synthesis with auxiliary classifier GANs," in *ICLR*, 2017.
- [3] R. D. Hjelm, A. P. Jacob, A. Trischler, G. Che, K. Cho, and Y. Bengio, "Boundary seeking GANs," in *ICLR*, 2018.
- [4] J.-Y. Zhu, R. Zhang, D. Pathak, T. Darrell, A. A. Efros, O. Wang, and E. Shechtman, "Toward multimodal image-to-image translation," in *NeurIPS*, 2017.
- [5] A. Brock, J. Donahue, and K. Simonyan, "Large scale GAN training for high fidelity natural image synthesis," in *ICLR*, 2019.
- [6] W. Jitkrittum, P. Sangkloy, M. W. Gondal, A. Raj, J. Hays, and B. Schölkopf, "Kernel mean matching for content addressability of GANs," in *ICML*, 2019.
- [7] E. Denton, S. Gross, and R. Fergus, "Semi-supervised learning with context-conditional generative adversarial networks," *arXiv preprint arXiv:1611.06430*, 2016.
- [8] M. Mirza and S. Osindero, "Conditional generative adversarial nets," *arXiv preprint arXiv:1411.1784*, 2014.
- [9] M.-Y. Liu and O. Tuzel, "Coupled generative adversarial networks," in *NeurIPS*, 2016.
- [10] K. Nazari, E. Ng, and M. Ebrahimi, "Image colorization using generative adversarial networks," in *AMDO*, 2018.
- [11] D. Pathak, P. Krahenbuhl, J. K. Donahue, T. Darrell, and A. A. Efros, "Context encoders: Feature learning by inpainting," in *CVPR*, 2016.
- [12] H. Zhang, Z. Zhang, A. Odena, and H. Lee, "Consistency regularization for generative adversarial networks," in *ICLR*, 2020.
- [13] J.-Y. Zhu, T. Park, P. Isola, and A. A. Efros, "Unpaired image-to-image translation using cycle-consistent adversarial networks," in *ICCV*, 2017.
- [14] M. Kang and J. Park, "ContraGAN: Contrastive learning for conditional image generation," in *NeurIPS*, 2020.
- [15] T. Kim, M. Cha, H. Kim, J. K. Lee, and J. Kim, "Learning to discover cross-domain relations with generative adversarial networks," in *ICML*, 2017.
- [16] H. Y. Lee, H. Y. Tseng, Q. Mao, J. B. Huang, Y. D. Lu, M. Singh, and M. H. Yang, "DRIT++: Diverse image-to-image translation via disentangled representations," *International Journal of Computer Vision*, vol. 128, no. 10-11, pp. 2402–2417, 2020.
- [17] Z. Yi, H. Zhang, P. Tan, and M. Gong, "DualGAN: Unsupervised dual learning for image-to-image translation," in *ICCV*, 2017.
- [18] J. Zhao, M. Mathieu, and Y. LeCun, "Energy-based generative adversarial networks," in *ICLR*, 2017.
- [19] X. Wang, K. Yu, S. Wu, J. Gu, Y. Liu, C. Dong, Y. Qiao, and C. Change Loy, "ESRGAN: Enhanced super-resolution generative adversarial networks," in *ECCV*, 2018.
- [20] A. Pumarola, A. Agudo, A. M. Martinez, A. Sanfeliu, and F. Moreno-Noguer, "GANimation: Anatomically-aware facial animation from a single image," in *ECCV*, 2018.
- [21] J. H. Lim and J. C. Ye, "Geometric GAN," *arXiv preprint arXiv:1705.02894*, 2017.
- [22] R. Sun, T. Fang, and A. Schwing, "Towards a better global loss landscape of GANs," *NeurIPS*, 2020.
- [23] Z. Zhao, S. Singh, H. Lee, Z. Zhang, A. Odena, and H. Zhang, "Improved consistency regularization for GANs," *arXiv preprint arXiv:2002.04724*, 2020.
- [24] X. Chen, Y. Duan, R. Houthoofd, J. Schulman, I. Sutskever, and P. Abbeel, "InfoGAN: Interpretable representation learning by information maximizing generative adversarial nets," in *NeurIPS*, 2016.
- [25] Y. Wu, J. Donahue, D. Balduzzi, K. Simonyan, and T. Lillicrap, "LOGAN: Latent optimisation for generative adversarial networks," *arXiv preprint arXiv:1912.00953*, 2019.
- [26] Y. Kim, M. Kim, and G. Kim, "Memorization precedes generation: Learning unsupervised GANs with memory networks," in *ICLR*, 2018.
- [27] X. Huang, M.-Y. Liu, S. Belongie, and J. Kautz, "Multimodal unsupervised image-to-image translation," in *ECCV*, 2018.
- [28] P. Isola, J.-Y. Zhu, T. Zhou, and A. A. Efros, "Image-to-image translation with conditional adversarial networks," in *CVPR*, 2017.
- [29] K. Bousmalis, N. Silberman, D. Dohan, D. Erhan, and D. Krishnan, "Unsupervised pixel-level domain adaptation with generative adversarial networks," in *CVPR*, 2017.
- [30] A. Jolicoeur-Martineau, "The relativistic discriminator: a key element missing from standard GAN," in *ICLR*, 2019.
- [31] A. Odena, "Semi-supervised learning with generative adversarial networks," in *ICMLW*, 2016.
- [32] M. Lin, "Softmax gan," *arXiv preprint arXiv:1704.06191*, 2017.
- [33] Y. Jin, J. Zhang, M. Li, Y. Tian, H. Zhu, and Z. Fang, "Towards the automatic anime characters creation with generative adversarial networks," *arXiv preprint arXiv:1708.05509*, 2017.
- [34] M.-Y. Liu, T. Breuel, and J. Kautz, "Unsupervised image-to-image translation networks," in *NeurIPS*, 2017.
- [35] M. Arjovsky and L. Bottou, "Towards principled methods for training generative adversarial networks," in *ICLR*, 2017.
- [36] I. Gulrajani, F. Ahmed, M. Arjovsky, V. Dumoulin, and A. Courville, "Improved training of wasserstein GANs," in *NeurIPS*, 2017.
- [37] N. Kodali, J. Abernethy, J. Hays, and Z. Kira, "On convergence and stability of GANs," *arXiv preprint arXiv:1705.07215*, 2017.
- [38] G. Daras, A. Odena, H. Zhang, and A. G. Dimakis, "Your local GAN: Designing two dimensional local attention mechanisms for generative models," in *CVPR*, 2020.
- [39] T. Karras, M. Aittala, J. Hellsten, S. Laine, J. Lehtinen, and T. Aila, "Training generative adversarial networks with limited data," in *NeurIPS*, 2020.
- [40] S. Nowozin, B. Cseke, and R. Tomioka, "f-GAN: training generative neural samplers using variational divergence minimization," in *NeurIPS*, 2016.

TABLE 3: Ground truth feature vector used for prediction of network architecture for all GMs. F1: # layers, F2: # convolutional layers, F3: # fully connected layers, F4: # pooling layers, F5: # normalization layers, F6: #filters, F7: # blocks, F8:# layers per block, F9: # parameters, F10: normalization type, F11: non-linearity type in last layer, F12: nonlinearity type in blocks, F13: up-sampling type, F14: skip connection, F15: downsampling

GM	F1	F2	F3	F4	F5	F6	F7	F8	F9	F10	F11	F12	F13	F14	F15
AAE	9	0	7	0	2	0	0	0	1593378	0	1	0	0	1	0
ACGAN	18	10	1	0	7	2307	5	3	4276739	0	1	1	0	1	0
ADAGAN_C	35	14	13	1	7	4131	9	3	9416196	0	1	1	0	1	0
ADAGAN_P	35	14	13	1	7	4131	9	3	9416196	0	1	1	0	1	0
ADV_FACES	45	23	1	1	20	2627	4	6	30000000	1	1	1	0	1	0
ALAE	33	25	8	0	0	4094	3	8	50200000	1	2	2	1	0	1
BEGAN	10	9	1	0	0	515	2	4	7278472	0	1	0	0	0	0
BETA_B	7	4	3	0	0	99	1	3	469173	3	3	1	0	1	1
BETA_H	7	4	3	0	0	99	1	3	469173	3	3	1	0	1	1
BETA_TCVAE	7	4	3	0	0	99	1	3	469173	3	3	1	0	1	1
BGAN	8	0	5	0	3	0	2	3	1757412	0	1	2	0	0	0
BICYCLE_GAN	25	14	1	0	10	4483	2	10	23680256	0	1	1	0	0	0
BIGGAN_128	63	21	1	0	41	6123	6	10	50400000	0	1	1	1	1	1
BIGGAN_256	75	25	1	0	49	7215	6	12	55900000	0	1	1	1	1	1
BIGGAN_512	87	29	1	0	57	8365	6	14	56200000	0	1	1	1	1	1
CADGAN	8	4	1	0	3	451	3	2	3812355	0	1	1	0	1	1
CCGAN	22	12	0	0	10	3203	2	9	29257731	0	1	1	1	1	1
CGAN	8	0	5	0	3	0	2	3	1757412	0	1	2	0	0	0
COCO_GAN	19	9	1	0	9	2883	3	4	50000000	0	1	1	0	0	0
COGAN	9	5	0	0	4	259	2	2	1126790	0	1	2	0	1	1
COLOUR_GAN	19	10	0	0	9	2435	2	9	19422404	0	1	1	0	1	1
CONT_ENC	19	11	0	0	8	5987	2	8	40401187	0	1	2	0	1	1
CONTRAGAN	35	14	13	1	7	4131	9	3	9416196	0	1	1	0	1	0
COUNCIL_GAN	62	30	3	0	29	6214	2	10	69616944	1	1	1	0	1	0
CRAMER_GAN	9	4	1	0	4	454	2	3	9681284	0	1	1	0	1	0
CRGAN_C	35	14	13	1	7	4131	9	3	9416196	0	1	1	0	1	0
CRGAN_P	35	14	13	1	7	4131	9	3	9416196	0	1	1	0	1	0
CYCLEGAN	47	24	0	0	23	2947	4	9	11378179	1	1	1	1	1	1
DAGAN_C	35	14	13	1	7	4131	9	3	9416196	0	1	1	0	1	0
DAGAN_P	35	14	13	1	7	4131	9	3	9416196	0	1	1	0	1	0
DCGAN	9	4	1	0	4	454	2	3	9681284	0	1	1	0	1	0
DEEPOOL	97	92	1	2	2	7236	4	10	22000000	2	0	1	1	0	0
DFCVAE	45	22	2	0	21	4227	4	7	2546234	0	3	2	0	0	1
DISCOGAN	21	12	0	0	9	3459	2	9	29241731	1	1	2	1	1	1
DRGAN	44	28	1	1	14	4481	3	8	18885068	0	1	0	0	1	1
DRIT	19	10	0	0	9	1793	4	3	9564170	1	1	1	1	1	1
DUALGAN	25	14	1	0	10	4483	2	10	23680256	0	1	1	0	0	0
EBGAN	6	3	1	0	2	195	2	2	738433	0	1	2	0	0	1
ESRGAN	68	66	0	0	2	4547	5	4	7012163	2	2	2	1	0	0
FACTOR_VAE	7	4	3	0	0	99	1	3	469173	3	3	1	0	1	1
FFGAN	39	19	1	1	19	3261	0	0	50000000	0	1	1	1	1	1
FGAN	5	0	3	0	2	0	2	2	2256401	0	3	1	0	1	0
FGAN_KL	5	0	3	0	2	0	2	2	2256401	0	3	1	0	1	0
FGAN_NEYMAN	5	0	3	0	2	0	2	2	2256401	0	3	1	0	1	0
FGAN_PEARSON	5	0	3	0	2	0	2	2	2256401	0	3	1	0	1	0
FGSM	97	92	1	2	2	7236	4	10	22000000	2	0	1	1	0	0
FPGAN	23	12	0	0	11	2179	2	6	53192576	1	1	1	0	0	1
FSGAN	37	20	0	1	16	2863	4	8	94669184	0	0	1	1	1	1
GAN_ANIME	25	18	0	0	7	2179	4	6	8467854	1	1	1	0	1	1
GDWCT	79	27	40	1	11	5699	2	4	51965832	1	1	1	0	0	1
GFLM	97	92	1	2	2	7236	4	10	22000000	2	0	1	1	0	0
GGAN	8	4	1	0	3	451	3	2	3812355	0	1	1	0	1	1
ICRGAN_C	35	14	13	1	7	4131	9	3	9416196	0	1	1	0	1	0
ICRGAN_P	35	14	13	1	7	4131	9	3	9416196	0	1	1	0	1	0
INFOGAN	7	3	1	0	3	195	2	2	1049985	0	1	2	0	0	1
LAPGAN	14	6	5	0	3	262	4	2	2182857	2	1	1	1	1	0
LOGAN	35	14	13	1	7	4131	9	3	9416196	0	1	1	0	1	0
LSGAN	9	5	0	0	4	1923	2	4	23909265	0	1	1	0	0	0
MAGAN	9	5	0	0	4	963	2	3	11140934	0	1	1	0	1	0
MEMGAN	14	7	1	0	6	1155	3	4	4128515	0	1	1	0	1	0
MMD_GAN	9	4	1	0	4	454	2	3	9681284	0	1	1	0	1	0
MRGAN	9	4	1	0	4	451	3	2	15038350	0	1	1	0	1	0
MSG_STYLE_GAN	33	25	8	0	0	4094	3	8	50200000	1	2	2	1	0	1
MUNIT	18	15	0	0	3	3715	2	6	10305035	1	0	1	1	1	1
OCFGAN	9	4	1	0	4	454	2	3	9681284	0	1	1	0	1	0
PGD	97	92	1	2	2	7236	4	10	22000000	2	0	1	1	0	0
PIX2PIX	29	16	0	0	13	5507	2	13	54404099	1	1	2	1	1	1
PIXELDA	27	14	1	0	12	835	4	6	483715	0	1	1	1	0	0
PROG_GAN	26	25	1	0	0	4600	3	8	46200000	0	3	3	0	0	1
RGAN	7	3	1	0	3	195	2	2	1049985	0	1	2	0	0	1
RSGAN_HALF	8	4	1	0	3	899	3	2	13129731	0	1	1	0	1	0
RSGAN_QUAR	8	4	1	0	3	451	3	2	3812355	0	1	1	0	1	0
RSGAN_REG	8	4	1	0	3	1795	3	2	48279555	0	1	1	0	1	0
RSGAN_RES_BOT	15	7	1	0	7	963	3	4	758467	0	1	1	1	1	0
RSGAN_RES_HALF	15	7	1	0	7	1155	3	4	1201411	0	1	1	1	1	0
RSGAN_RES_QUAR	15	7	1	0	7	579	3	4	367235	0	1	1	1	1	0
RSGAN_RES_REG	15	7	1	0	7	2307	3	4	4270595	0	1	1	1	1	0
SAGAN	11	6	1	0	4	139	2	4	16665286	0	1	2	0	0	0
SEAN	19	16	0	0	0	5062	2	7	266907367	3	1	1	0	1	0
SEMANTIC	23	12	0	0	11	2179	2	6	53192576	1	1	1	0	0	1
SGAN	7	3	1	0	3	195	2	2	1049985	0	1	2	0	0	1
SNGAN	23	11	1	0	11	3871	4	5	10000000	0	1	1	0	1	0
SOFT_GAN	8	0	5	0	3	0	2	3	1757412	0	1	2	0	0	0
SRRNET	74	36	1	0	37	2819	4	16	4069955	0	1	1	0	1	1
STANDARD_VAE	7	4	3	0	0	99	1	3	469173	3	3	1	0	1	1
STARGAN	23	12	0	0	11	2179	2	6	53192576	1	1	1	0	0	1
STARGAN_2	67	26	12	4	25	4188	4	12	94008488	1	2	2	0	0	1
STGAN	19	10	0	0	9	2953	2	5	25000000	0	1	2	1	1	1
STYLEGAN	33	25	8	0	0	4094	3	8	50200000	1	2	2	1	0	1
STYLEGAN_2	33	25	8	0	0	4094	3	8	59000000	1	2	2	1	0	1
STYLEGAN2_ADA	33	25	8	0	0	4094	3	8	59000000	1	2	2	1	0	1
TPGAN	45	31	2	1	11	5275	0	0	27233200	0	3	3	0	1	1
UGAN	9	4	1	0	4	771	2	3	4850692	0	3	1	0	1	0
UNIT	43	22	0	0	21	4739	4	8	13131779	1	1	1	1	1	1
VAEGAN	17	7	2	0	8	867	2	6	26396740	0	1	1	0	0	1
WGAN	9	5	0	0	4	1923	2	4	23909265	0	1	1	0	0	0
WGAN_DRA	18	10	1	0	7	2307	5	3	4276739	0	1	1	0	1	0
WGAN_WC	18	10	1	0	7	2307	5	3	4276739	0	1	1	0	1	0
WGANP	9	5	0	0	4	1923	2	4	23905841	0	1	1	0	0	0
YLG	33	20	1	2	10	5155	5	5	42078852	0	1	1	1	1	1

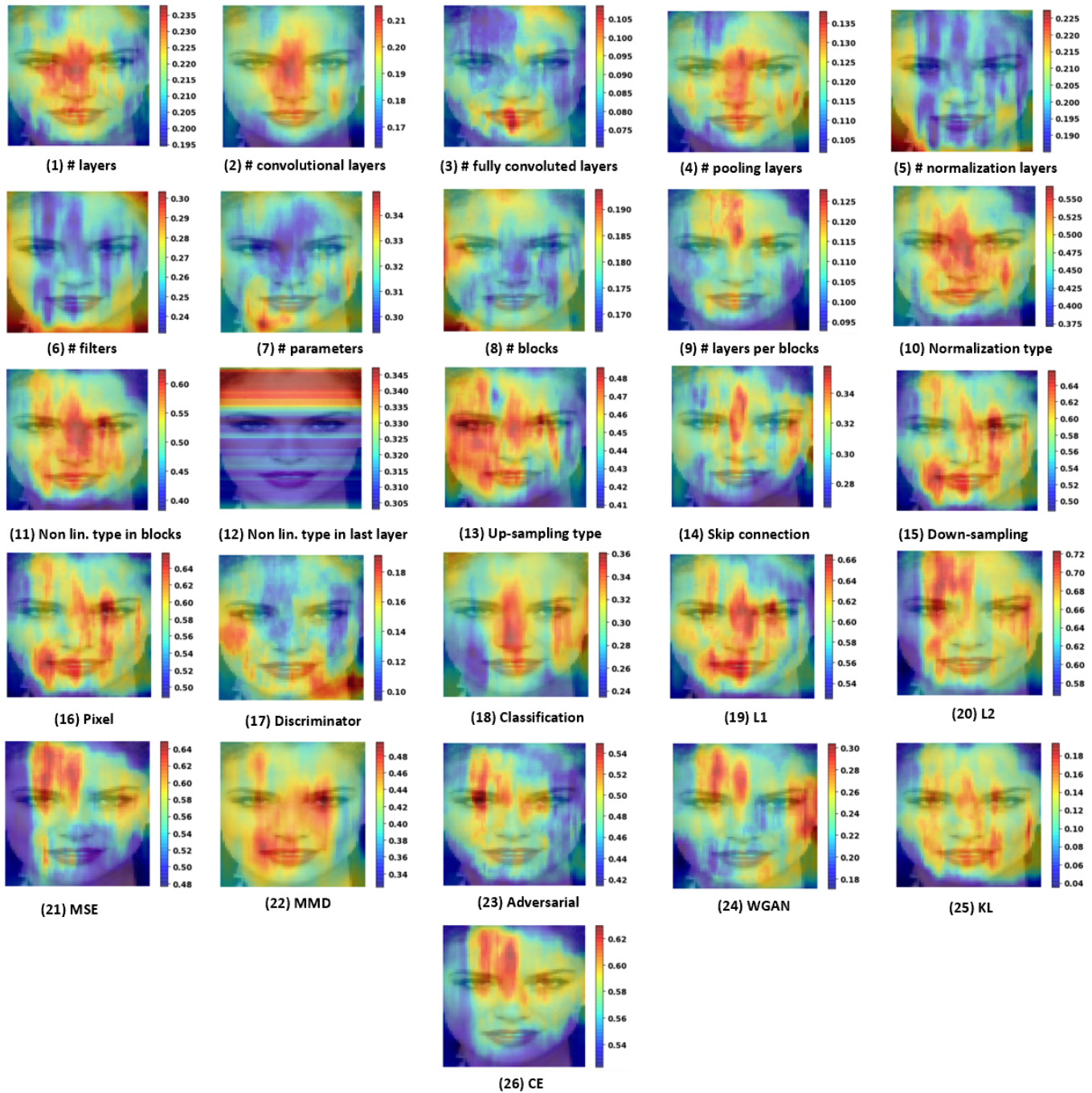


Fig. 1: Feature heatmap for each feature in network architecture and loss function predicted feature vector for face data. Each heatmap provides the importance of the region in the estimation of the respective parameter.

[41] E. Denton, S. Chintala, A. Szlam, and R. Fergus, "Deep generative image models using a laplacian pyramid of adversarial networks," in *NeurIPS*, 2015.

[42] L. Metz, B. Poole, D. Pfau, and J. Sohl-Dickstein, "Unrolled generative adversarial networks," in *ICLR*, 2017.

[43] T. Karras, M. Aittala, J. Hellsten, S. Laine, J. Lehtinen, and T. Aila, "Training generative adversarial networks with limited data," in *NeurIPS*, 2020.

[44] X. Mao, Q. Li, H. Xie, R. Y. Lau, Z. Wang, and S. Paul Smolley, "Least squares generative adversarial networks," in *ICCV*, 2017.

[45] M. Arjovsky, S. Chintala, and L. Bottou, "Wasserstein generative adversarial networks," in *ICML*, 2017.

[46] O. Nizan and A. Tal, "Breaking the cycle - colleagues are all you need," in *CVPR*.

[47] T. Xiao, J. Hong, and J. Ma, "DNA-GAN: Learning disentangled representations from multi-attribute images," *ICLRW*, 2018.

[48] M. M. Rahman Siddiquee, Z. Zhou, N. Tajbakhsh, R. Feng, M. B. Gotway, Y. Bengio, and J. Liang, "Learning fixed points in generative adversarial networks: From image-to-image translation to disease detection and localization," in *ICCV*, 2019.

[49] W. Cho, S. Choi, D. K. Park, I. Shin, and J. Choo, "Image-to-image translation via group-wise deep whitening-and-coloring transformation," in *CVPR*, 2019.

[50] A. Karnewar and O. Wang, "MSG_GAN: Multi-scale gradients for generative adversarial networks," in *CVPR*, 2020.

[51] S. Pidhorskyi, D. A. Adjeroh, and G. Doretto, "Adversarial latent autoencoders," in *CVPR*, 2020.

[52] N. Papernot, F. Faghri, N. Carlini, I. Goodfellow, R. Feinman, A. Kurakin, C. Xie, Y. Sharma, T. Brown, A. Roy, A. Matyasko, V. Behzadan, K. Hambardzumyan, Z. Zhang, Y.-L. Juang, Z. Li, R. Sheatsley, A. Garg,



Fig. 2: Feature heatmap for each feature in network architecture and loss function predicted feature vector for MNIST data.

J. Uesato, W. Gierke, Y. Dong, D. Berthelot, P. Hendricks, J. Rauber, and R. Long, "Technical report on the cleverhans v2.1.0 adversarial examples library," *arXiv preprint arXiv:1610.00768*, 2018.

[53] D. Deb, J. Zhang, and A. K. Jain, "Advfaces: Adversarial face synthesis," in *IJCB*, 2019.

[54] A. Dabouei, S. Soleymani, J. Dawson, and N. Nasrabadi, "Fast geometrically-perturbed adversarial faces," in *WACV*, 2019.

[55] H. Qiu, C. Xiao, L. Yang, X. Yan, H. Lee, and B. Li, "Semanticadv: Generating adversarial examples via attribute-conditioned image editing," in *ECCV*, 2020.

[56] A. Madry, A. Makelov, L. Schmidt, D. Tsipras, and A. Vladu, "Towards deep learning models resistant to adversarial attacks," in *ICLR*, 2018.

[57] X. Yuan, P. He, Q. Zhu, and X. Li, "Adversarial examples: Attacks and defenses for deep learning," *IEEE transactions on neural networks and learning systems*, vol. 30, no. 9, pp. 2805–2824, 2019.

[58] S.-M. Moosavi-Dezfooli, A. Fawzi, and P. Frossard, "DeepFool: a simple and accurate method to fool deep neural networks," in *CVPR*, 2016.

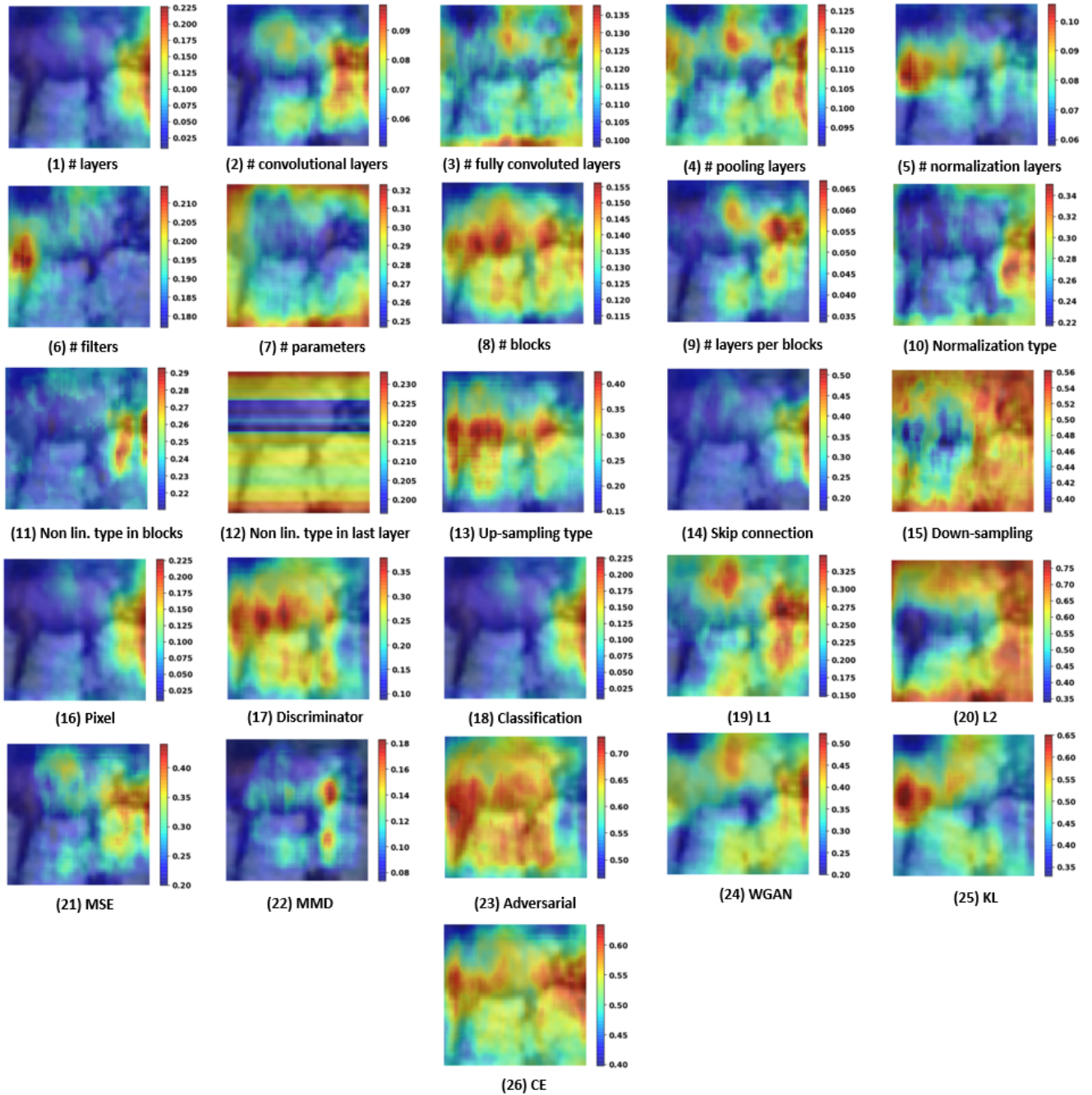


Fig. 3: Feature heatmap for each feature in network architecture and loss function predicted feature vector for CIFAR data.

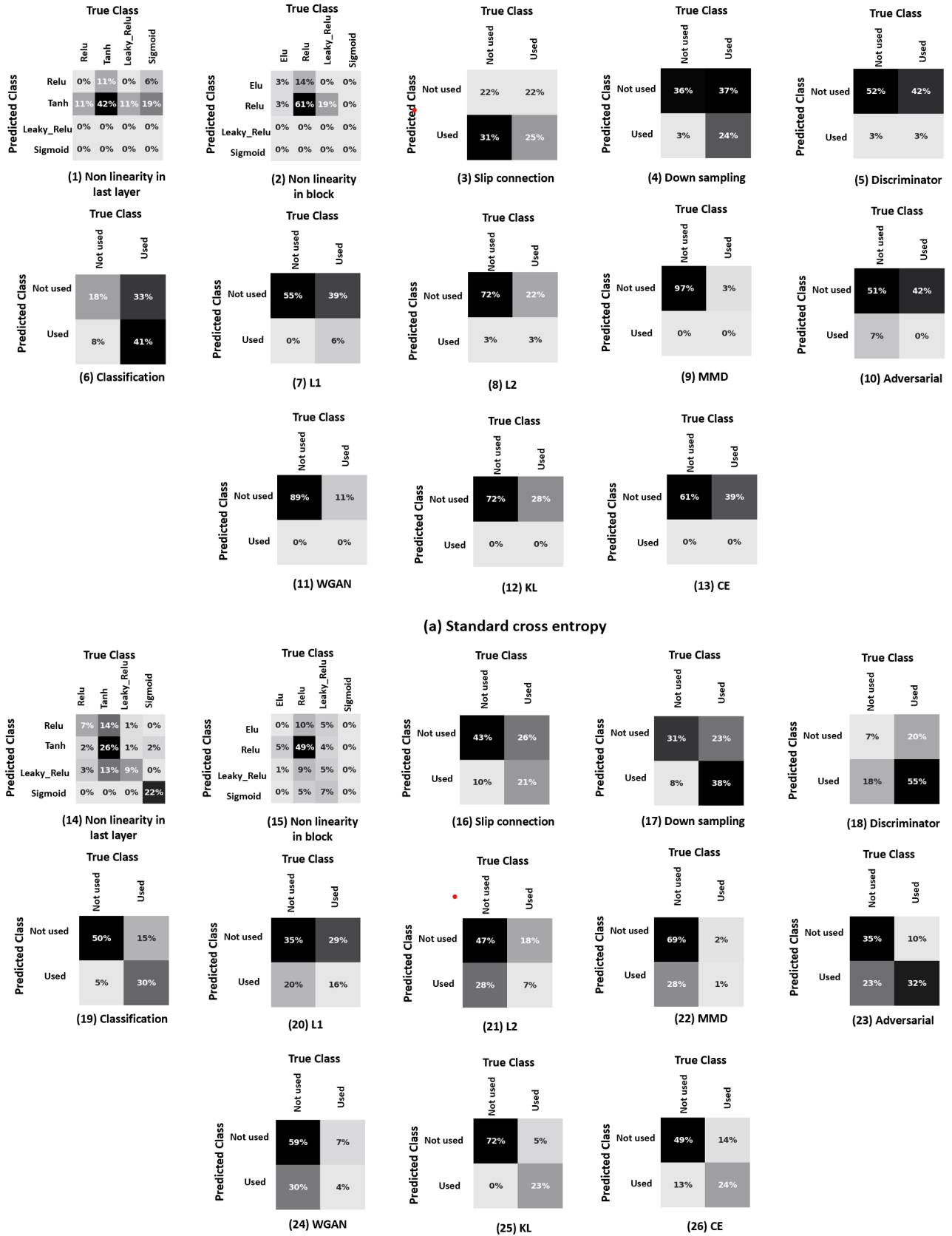


Fig. 4: Confusion matrix in the estimation of remaining parameters which were not shown in paper for network architecture and loss function. (1)-(13): Standard cross-entropy and (14)-(26): Weighted cross entropy. Weighted cross entropy handles imbalance of data much better than the standard cross entropy which usually predicts one class.

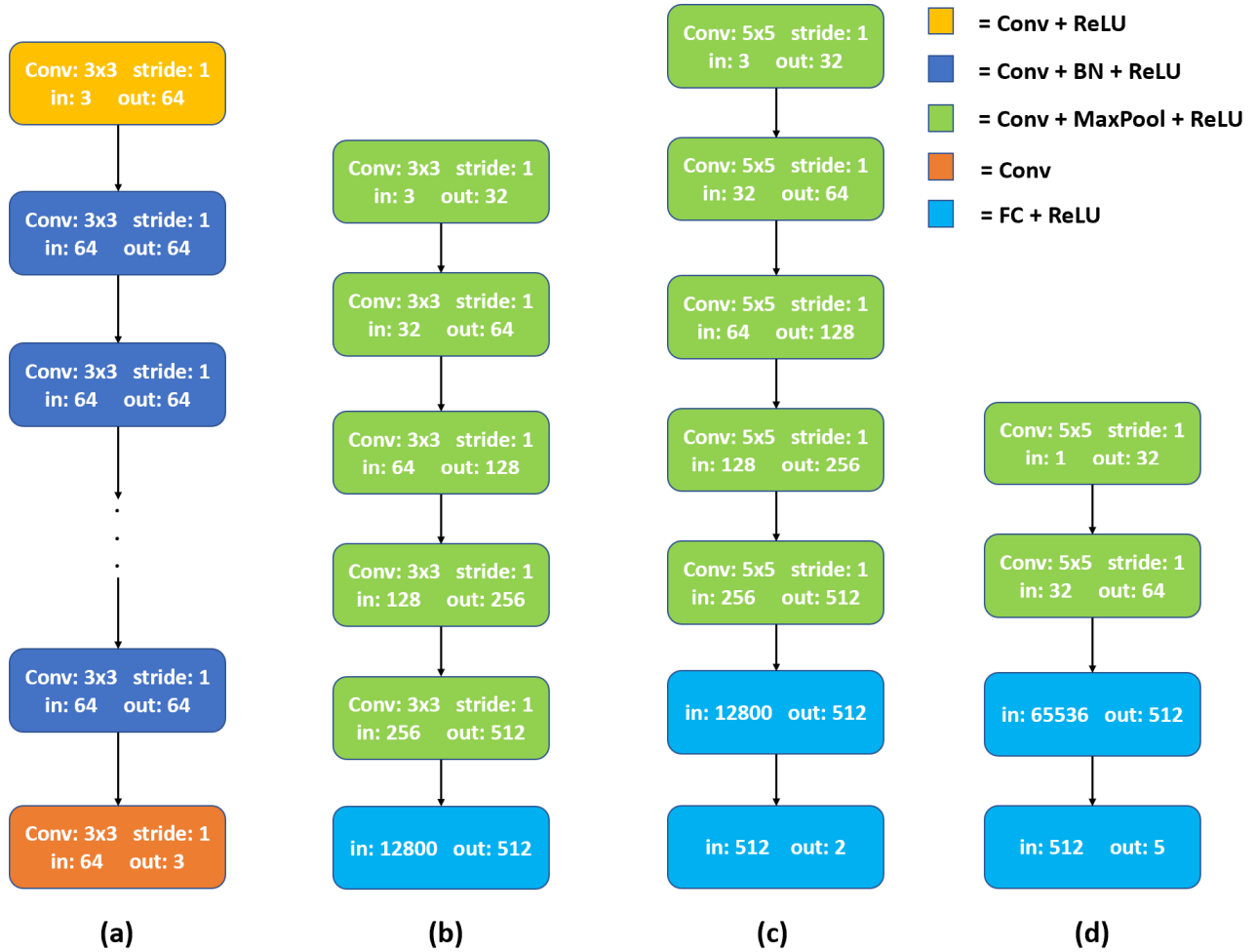


Fig. 5: Network architecture for various components of our method. (a) FEN (b) Encoder in PN (c) Shallow network for deepfake detection (d) Shallow network for image attribution.

TABLE 4: Feature value for different labels of multi-class and binary features.

Feature	Label	Value
F10	0	Batch Normalization
	1	Instance Normalization
	2	Adaptive Instance Normalization
	3	No Normalization
F11	0	ReLU
	1	Tanh
	2	Leaky_ReLU
	3	Sigmoid
F12	0	ELU
	1	ReLU
	2	Leaky_ReLU
	3	Sigmoid
F13	0	Nearest Neighbour
	1	Deconvolution
F14 and F15	0	Feature used
	1	Feature not used

TABLE 5: Feature value for different labels of multi-class and binary features.

Feature	Label	Value
Normalization type	0	Batch Normalization
	1	Instance Normalization
	2	Adaptive Instance Normalization
	3	No Normalization
Non-linearity type in last layer	0	ReLU
	1	Tanh
	2	Leaky_ReLU
	3	Sigmoid
Non-linearity type in blocks	0	ELU
	1	ReLU
	2	Leaky_ReLU
	3	Sigmoid
Upsampling type	0	Nearest Neighbour
	1	Deconvolution
Skip connection and downsampling	0	Feature used
	1	Feature not used

TABLE 6: Ground truth feature vector used for prediction of loss type for all GMs.

GM	L_1	L_2	MSE	MMD	WGAN	KL	Adversarial	CE
AAE	1	0	0	0	0	0	0	1
ACGAN	1	0	0	0	0	0	0	1
ADAGAN_C	0	0	0	0	1	0	0	1
ADAGAN_P	0	0	0	0	1	0	0	0
ADV_FACES	1	0	1	0	1	0	0	0
ALAE	0	0	1	0	1	0	0	0
BEGAN	1	0	0	0	0	0	0	0
BETA_B	0	0	0	0	0	0	1	0
BETA_H	0	0	0	0	0	0	1	1
BETA_TCVAE	1	0	0	0	0	0	1	1
BGAN	0	0	0	0	1	0	0	1
BICYCLE_GAN	1	0	1	0	0	0	1	0
BIGGAN_128	1	0	0	0	0	0	0	0
BIGGAN_256	1	0	0	0	0	0	0	0
BIGGAN_512	1	0	0	0	0	0	0	0
CADGAN	0	0	0	1	0	0	0	0
CCGAN	0	0	0	0	1	0	0	0
CGAN	0	0	1	0	1	0	0	0
COCO_GAN	1	1	0	0	0	1	0	0
COGAN	0	0	0	0	1	0	0	0
COLOUR_GAN	1	0	0	0	1	0	0	0
CONT_ENC	0	1	0	0	1	0	0	0
CONTRAGAN	1	0	0	0	1	0	0	1
COUNCIL_GAN	1	0	1	0	1	0	0	0
CRAMER_GAN	0	0	0	0	0	1	0	0
CRGAN_C	1	1	0	0	0	0	0	1
CRGAN_P	1	1	0	0	0	0	0	0
CYCLEGAN	1	0	0	0	1	0	0	0
DAGAN_C	1	0	0	0	0	0	0	1
DAGAN_P	1	0	0	0	0	0	0	0
DCGAN	0	0	0	0	0	0	0	1
DEEPFOOL	1	1	0	0	0	0	0	0
DFCVAE	0	1	0	0	0	0	1	1
DISCOGAN	1	0	0	0	1	0	0	0
DRGAN	0	0	0	0	1	0	0	1
DRIT	1	0	0	0	1	0	0	1
DUALGAN	1	0	0	0	0	1	0	0
EBGAN	0	1	0	0	1	0	0	0
ESRGAN	1	0	0	0	1	0	0	0
FACTOR_VAE	1	0	0	0	1	0	0	1
FFGAN	1	1	0	0	1	0	0	1
FGAN	0	0	0	0	1	0	0	0
FGAN_KL	1	0	0	0	0	0	0	0
FGAN_NEYMAN	0	1	0	0	0	0	0	0
FGAN_PEARSON	0	0	1	0	0	0	0	0
FGSM	0	0	0	0	1	0	0	0
FPGAN	1	1	0	0	1	0	0	1
FSGAN	1	0	0	0	1	0	0	1
GAN_ANIME	1	1	0	0	0	1	0	0
GDWCT	1	0	1	0	0	0	0	0
GFLM	0	0	1	0	0	0	0	1
GGAN	1	0	0	0	0	0	0	0
ICRGAN_C	1	1	0	0	0	0	0	1
ICRGAN_P	1	1	0	0	0	0	0	0
INFOGAN	0	0	1	0	1	0	0	1
LAPGAN	0	0	0	0	1	0	0	0
LOGAN	1	0	0	0	0	0	0	0
LSGAN	0	0	1	0	0	0	0	0
MAGAN	0	0	1	0	0	0	0	0
MEMGAN	0	0	0	0	1	0	0	0
MMD_GAN	1	0	0	1	0	0	0	0
MRGAN	0	0	1	0	1	0	0	0
MSG_STYLE_GAN	0	0	0	0	1	0	0	0
MUNIT	1	0	0	0	1	0	0	0
OCFGAN	0	0	0	1	0	0	0	0
PGD	1	1	0	0	0	0	0	0
PIX2PIX	1	0	0	0	1	0	0	0
PIXELDA	0	0	0	0	1	0	0	1
PROG_GAN	0	0	0	0	0	1	0	0
RGAN	0	0	0	0	0	1	0	0
RSGAN_HALF	0	0	0	0	0	0	0	1
RSGAN_QUAR	0	0	0	0	0	0	0	1
RSGAN_REG	0	0	0	0	0	0	0	1
RSGAN_RES_BOT	0	0	0	0	0	0	0	1
RSGAN_RES_HALF	0	0	0	0	0	0	0	1
RSGAN_RES_QUAR	0	0	0	0	0	0	0	1
RSGAN_RES_REG	0	0	0	0	0	0	0	1
SAGAN	0	0	0	0	1	0	0	0
SEAN	1	0	0	0	1	0	0	0
SEMANTIC	0	1	0	0	1	0	0	0
SGAN	0	0	0	0	1	0	0	1
SNGAN	0	0	0	0	1	0	0	0
SOFT_GAN	0	0	0	0	1	0	0	0
SRRNET	0	1	1	0	1	0	0	1
STANDARD_VAE	0	0	0	0	1	0	0	1
STARGAN	1	0	0	0	1	0	0	1
STARGAN_2	1	0	0	0	1	0	0	0
STGAN	1	0	0	0	1	1	0	0
STYLEGAN	0	1	0	0	0	1	0	0
STYLEGAN_2	0	1	0	0	1	0	0	0
STYLEGAN2_ADA	0	1	0	1	1	0	0	0
TPGAN	1	0	0	0	0	1	0	0
UGAN	0	0	0	0	1	0	0	0
UNIT	0	0	0	0	1	0	1	0
VAEGAN	1	0	0	0	1	0	1	0
WGAN	0	0	0	0	0	1	0	0
WGAN_DRA	0	0	1	0	0	1	0	0
WGAN_WC	0	0	0	0	0	1	0	0
WGANP	0	1	0	0	0	1	0	0
YLG	0	0	0	0	0	1	0	0